Review

Cobalt-Rich Fe-Mn Crusts in the Western Pacific Magellan Seamount Trail: Geochemistry and Chronostratigraphy

Igor S. Peretyazhko *, Elena A. Savina, Irina A. Pulyaeva

Posted Date: 21 October 2025

doi: 10.20944/preprints202510.1578.v1

Keywords: Cobalt-rich Fe-Mn crusts; geochemistry; chronostratigraphy; biostratigraphy; calcareous nannofossils; Govorov; Kocebu and Pallada guyots; Magellan Seamount Trail

Review

Cobalt-Rich Fe-Mn Crusts in the Western Pacific Magellan Seamount Trail: Geochemistry and Chronostratigraphy

Igor S. Peretyazhko [1,*], Elena A. Savina [1] and Irina A. Pulyaeva [1,2]

[1] Vinogradov Institute of Geochemistry, Russian Academy of Sciences, Siberian Branch, 664033 Irkutsk, Russia

[2] JSC Yuzhmorgeologiya, 353461 Gelendzhik, Russia

* Correspondence: pgmigor@igc.irk.ru

Abstract

Synthesis of published and new data from Govorov and Kocebu guyots provides geochemical and chronostratigraphic constraints on hydrogenetic cobalt-rich Fe-Mn crusts from the Western Pacific Magellan Seamount Trail (MST). The history of the crusts began about 65–60 Myr ago, when the relict layer R was deposited in the Campanian–Maastrichtian and Late Paleocene along the shores of guyots. The growth of the old-generation crusts continued in the Late Paleocene–Early Eocene (Layer I-1) and in the Middle–Late Eocene (Layer I-2) in a shallow-water shelf environment. The younger layers of crusts formed in the Late Oligocene–Early Miocene (Layer I-2b), Miocene (Layer II), and Pliocene–Pleistocene (Layer III) at depths about the present sealevel. The precipitation of Fe and Mn oxyhydroxides from seawater was interrupted by several episodes of dissolution, the longest one between the old and young layers of Fe-Mn crusts (from 38 to 26.5 Ma). Fe and Mn oxyhydroxides in the crusts were affected by two global events of phosphogenesis in the Pacific: Late Eocene–Early Oligocene, from 43 to 39 Ma (Layers R, I-1, I-2) and Late Oligocene–Early Miocene, from 27 to 21 Ma (Layer I-2b). The trace element patterns in different layers of the Fe-Mn crusts are grouped using factor analysis of principal components (varimax raw) into four factors: (1) + (all REEs except Ce and La); (2) +(Ce, La, Ba, Mo, Sr, Pb); (3) +(Zr, Hf, Nb, Rb, As)/-Pb; (4) +(U, Th, Co, As, Sb, W)/-Y. The factor score diagrams highlight fields which are especially contrasting for Layers I-1, I-2 and II+III according to factors 2 and 4. Consistent REE and Y variations in Layers I-2b→II →III of the crust from Pallada Guyot correlate with gradual ocean deepening between the Late Oligocene–Early Miocene and Present when the MST guyots were submerging. Large variations in trace element contents across coeval layers may be due to hydrodynamics of currents on the guyot surfaces. Furthermore, the geochemistry of the crusts bears effects from repeated episodes of Cenozoic volcanism in the MST region of the Pacific Plate. Higher contents of Nb, Zr, As, Sb, and W in the younger layers II and III may result from large-scale volcanism, including Miocene eruptions of petit-spot volcanoes.

Keywords: Cobalt-rich Fe-Mn crusts; geochemistry; chronostratigraphy; biostratigraphy; calcareous nannofossils; Govorov; Kocebu and Pallada guyots; Magellan Seamount Trail

1. Introduction

Cobalt-rich ferromanganese crusts on guyots and seamounts are attractive exploration targets having significant mineral potential, including critical metals and other valuable elements (Co, Ni, Cu, Mn, Zr, Mo, W, REEs and Y, etc.) [1–8]. The Magellan Seamount Trail in the Pacific Ocean, one of best documented exploration regions, comprises seventeen flat-topped guyots and several relatively small seamounts with peak-like summits. The names of the MST guyots were approved by the IHO-IOC GEBCO Gazetteer of Undersea Feature Names (available online at http://www.ngdc.noaa.gov/gazetteer/) and are recommended for use in all relevant publications.

 doi:10.20944/preprints202510.1578.v1

Many of the guyots were named after Russian scientists who contributed a lot into the research of oceans as a whole and Fe-Mn crusts or nodules in particular (I.N. Govorov, N.S. Skornyakova, V.M. Gordin, V.I. Il'ichev, K.N. Fedorov, I.S. Gramberg, L.K. Zatonsky, M.E. Melnikov, and E.L. Shkolnik), and sea explorers I.I. Butakov and O.E. Kocebu. The names of four guyots refer to Russian ships: frigate *Pallada*, most noted for studies of the Far East, as well as modern research vessels *Pegas*, *Vulkanolog*, and *Gelendzhik* used in numerous cruises over the MST region.

Main results, including geological and geophysical maps of the region, lithology, mineralogy, and chemistry of volcanic rocks and Fe-Mn crusts are available at http://guyot.ocean.ru, in technical reports of JSC *Yuzhmorgeologiya*, and in a number of publications [9–21]. Cobalt-rich Fe-Mn crusts (Fe-Mn crusts or crusts hereafter) in many MST guyots have been largely documented in terms of occurrence, stratigraphy, zoning, mineralogy, and chemistry in the course of cruises by teams from Russia, China, South Korea, Japan, and other countries. Exploration for crusts in Govorov, Kocebu, Alba, and Vulkanolog guyots (scale 1:50 000) has been carried out by JSC *Yuzhmorgeologiya* surveys since 2015 on contract with the International Seabed Authority, https://isa.org.jm/exploration-contracts/cobalt-rich-ferromanganese-crusts/.

The ~1200 km long Magellan Seamount Trail (MST) comprises Govorov, Skornyakova, Gordin, Vulkanolog, Kocebu, Alba, Il'ichev, Shkolnik, Pegas, Pallada, and Melnikov guyots in the northwestern flank and Fedorov, Ita Mai Tai, Gelendzhik, Gramberg, Zatonsky, Butakov, and Arirang guyots in the southeast (Figure 1). The bases of the volcanic edifices lie at sea depths from 5100–5300 m in the northwest to 5500–5900 m in the southeast of MST. Many guyots are extended with small satellite edifices and numerous offshoots. Their flat summit plateaus reach depths from 1400–1600 m to 2000–2600 m below the sealevel. The guyots are composed of Cretaceous alkali-basaltic and volcaniclastic rocks [9–11]. Events of Cenozoic volcanic activity in the Pacific Plate produced multiple volcanic cones and domes rising above the summit plateaus of Govorov, Alba, Kocebu and other guyots [12,13,18,19]. For example, Cenozoic eruption products found on Alba Guyot include basanites and tuffs of Miocene petit-spot volcanoes [14,20,21]. The guyot summit plateaus occurred at shallow sea depths till the latest Eocene and submerged to about the present bathymetric level in Oligocene–Miocene–Pliocene time [9–12]. Co-rich Fe-Mn crusts precipitated on hard rock substrates along the periphery of the summit plateaus and slopes till the 3000–3500 m sea depths but are absent from sediment-covered low-angle slopes deeper than 3500 m. The thickness of the crusts varies from 14–15 cm in the northwestern MST guyots to 20–25 cm in the southeastern guyots. The thickest crusts (up to 40 cm) were reported from Ita Mai Tai Guyot [22].

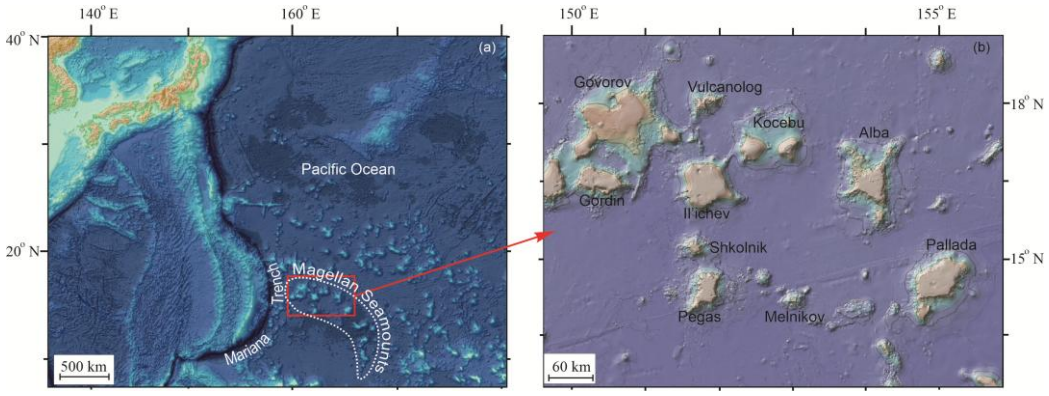

Figure 1. Magellan Seamounts in the Pacific (a) and guyots in the northwestern MST flank (b) from https://maps.ngdc.noaa.gov/viewers/bathymetry/.

1.1. Morphology and Mineralogy of Fe-Mn Crusts

The structure, texture, and mineralogy features of the MST hydrogenetic Co-rich Fe-Mn crusts were detailed in multiple Russian publications [9–12,22–32].

 doi:10.20944/preprints202510.1578.v1

Few crust samples (23%) contain fragments of the mosaic laminated relict layer (R) containing numerous microinclusions and round inclusions of carbonate fluorapatite (CFA) near the top. The layer is crosscut by 5–8 mm veinlets with phosphate or argillic fill (Figure 2).

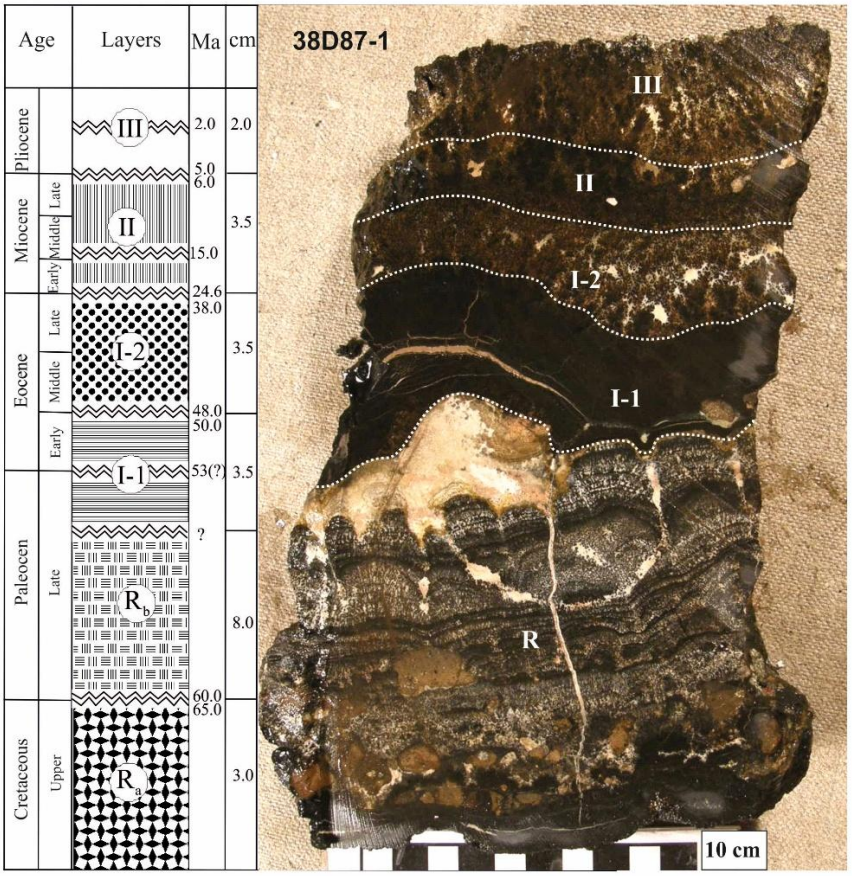

Figure 2. Generalized section of MST Co-rich Fe-Mn crusts, after [9,23,24] and an example of a full section of crust from the Butakov Guyot (sample 37D87-1).

The complete sections of most crusts begin with a dense black laminated layer (I-1) of 90 to 220 quasi-parallel laminas per 1 cm. The ore material is bluish black on the cleavage plane, with diamond luster, conchoidal fracture, and occasionally with flaky jointing. The space between laminas, as well as numerous 0.01–0.3 mm (rarely up to 1–2 mm) thick crosscutting veinlets, are filled with whitish or yellowish CFA aggregate bearing phosphatized nannofossils and foraminifers.

The basal layer is overlain by Layer I-2, which is similar to Layer I-1 in the degree of ore alteration but is poorer in CFA. The layer looks mottled due to a combination of black columns, Fe-Mn globules, and CFA inclusions. Locally, some 1–3 cm fragments show blind jointing. The boundary with Layer I-1 below is commonly smooth but is sometimes sharp. Layers I-1 and I-2 are discordant in some sections.

Layer II has a radiated-columnar structure, with roughly parallel columns of Fe and Mn oxyhydroxides perpendicular to the layer boundaries, branching in the upper part, and argillic material in the interstitial space. Porous zones bear a gravel mixture of small rock and mineral grain clasts, foraminifers, and calcareous nannoplankton. The layer encloses carbonate-clayey and carbonate-phosphate lenses in the bottom part. Layers II-1 and II-2 are sometimes clearly distinguishable. The boundary with the underlying Layer I-2 is sharp, often with an angular unconformity.

The uppermost Layer III has a heterogeneous general appearance, a massive structure, and a variable thickness. Its brownish-black color is due to fine ochreous particles disseminated among the

 doi:10.20944/preprints202510.1578.v1

black ore material. The boundary between Layers III and II may be either very sharp or smooth. Fe and Mn oxyhydroxides in Layers II and III bear no evident signatures of postdepositional alteration.

Thus, the complete section of Fe-Mn crusts from the MST guyots comprises five units: R (rarely found) → I-1 → I-2 → II → III. However, most of the sections are reduced to fewer layers (I-1 → II → III; I-2 → II → III; II → III), and often to single Layer III few cm thick (more than 50% of all related crust fields on the guyot surfaces).

The mineralogy of the crusts is rather uniform [9–11,22,30–33] and consists of two dominant ore-forming components and various phases occurring in minor amounts. The main phases are poorly crystalline Fe-vernadite (δ-MnO_2) and X-ray amorphous Mn-bearing iron oxyhydroxide with a feroxyhyte (δ-FeOOH) structure in all layers. Other phases include buserite, asbolane-buserite, todorokite (10Å phase), birnessite (7Å phase), pyrolusite, romanechite, iron hydroxides (goethite, akaganeite, lepidocrocite, hematite), lithiophorite, Ca-psilomelane (rancieite), and other rarer phases.

The mineralogy of the oldest relict layer R differs markedly from that of the younger layers in the presence of asbolane (or asbolane-buserite with abundant asbolane wads), disseminated goethite, as well as lesser percentages of Fe-vernadite, feroxyhyte, ferrihydrite, and ubiquitous todorokite.

Non-metallic phases are unevenly distributed across the crusts: mainly CFA enclosing <1 μm sized cerianite, parisite, monazite, bastnaesite, barite, and other phases in Layers I-1, I-2, while Layer II contains inclusions or aggregates of montmorillonite-illite, chlorite, zeolites (phillipsite or rarely heulandite and analcime), detrital plagioclase, K-Na feldspar, clinopyroxene (diopside-hedenbergite), and amphibole (hastingsite, tremolite). Different layers bear inclusions of biogenic calcite, veinlets or inclusions of abiogenic calcite and rarely aragonite, siderite, and dolomite, as well as abundant quartz in Layer III.

1.2. Formation History of Fe-Mn Crusts

The history and ages of layers in the complete section of MST Fe-Mn crusts (Figure 2) were reconstructed from index species of calcareous nannoplankton, as well as identified foraminifers, radiolarians, and macrofossils (molluscs and corals) with reference to the stratigraphy of guyots and main paleogeographic events in the ocean from the Late Cretaceous to the Cenozoic [9–12,23–29].

The oldest relict Layer R was deposited in the Campanian–Maastrichtian (sublayer Ra) and Paleocene (sublayer Rb), in shallow water near the shore, probably within the photic zone. The precipitation continued in the Late Paleocene-Early Eocene, in a relatively shallow shelf environment, at sea depths <500–600 m (Layer I-1), and in the Middle–Late Eocene (Layer I-2). Layer II was deposited in the Late Oligocene–Miocene at sea depths of 1200–3000 m, close to the present sealevel, while Layer III formed in Pliocene–Pleistocene time.

Thin layers and pores in the ore component of old layers R, I-1, and I-2 are filled with phosphatized biogenic carbonate partly replaced by CFA. The crusts became enriched with phosphorus and crystallized CFA after the deposition of old layers during the Late Eocene–Early Oligocene (43–39, with a peak at 37 Ma) and Late Oligocene–Early Miocene (27–21 Ma) global events of phosphogenesis in the Pacific [34]. The phosphogenic reactions mobilized and redistributed minor and trace elements between Fe-Mn oxyhydroxides and phosphate matter and induced crystallization of CFA, REE carriers, asbolane-buserite, and other phases [11,35–38]).

The stages of precipitation and growth in the history of the Fe-Mn crusts were interrupted by local paleoceanographic events: (1) partial dissolution of previously deposited layers under global and regional changes in the compositions, redox conditions, and physical parameters of seawater; (2) hydrodynamic changes in currents on the guyot surfaces; (3) sediment deposition; (4) volcaniclastic deposition during episodes of volcanic activity. The longest gap (up to 12-14 Myr) separated the old (R, I-1, I-2) and young (II, III) generations of the crust layers (Figure 2).

Many MST guyots and seamounts in the Pacific tropical latitudes share the features of morphology, mineralogy, and formation history of hydrogenetic Fe-Mn crusts [26–29], which is evidence of extensive Late Cretaceous–Cenozoic precipitation of Fe and Mn oxyhydroxides from seawater over a large territory of the equatorial Pacific for at least 60–65 Myr. As an example, Figure

 doi:10.20944/preprints202510.1578.v1

3 shows identified index species of calcareous nannofossils in two crusts from Butakov and Lomilik (Marshall Islands) guyots, after [29]. Unlike the section of Figure 2, these sections include Late Oligocene–Early Miocene Layer I-2b.

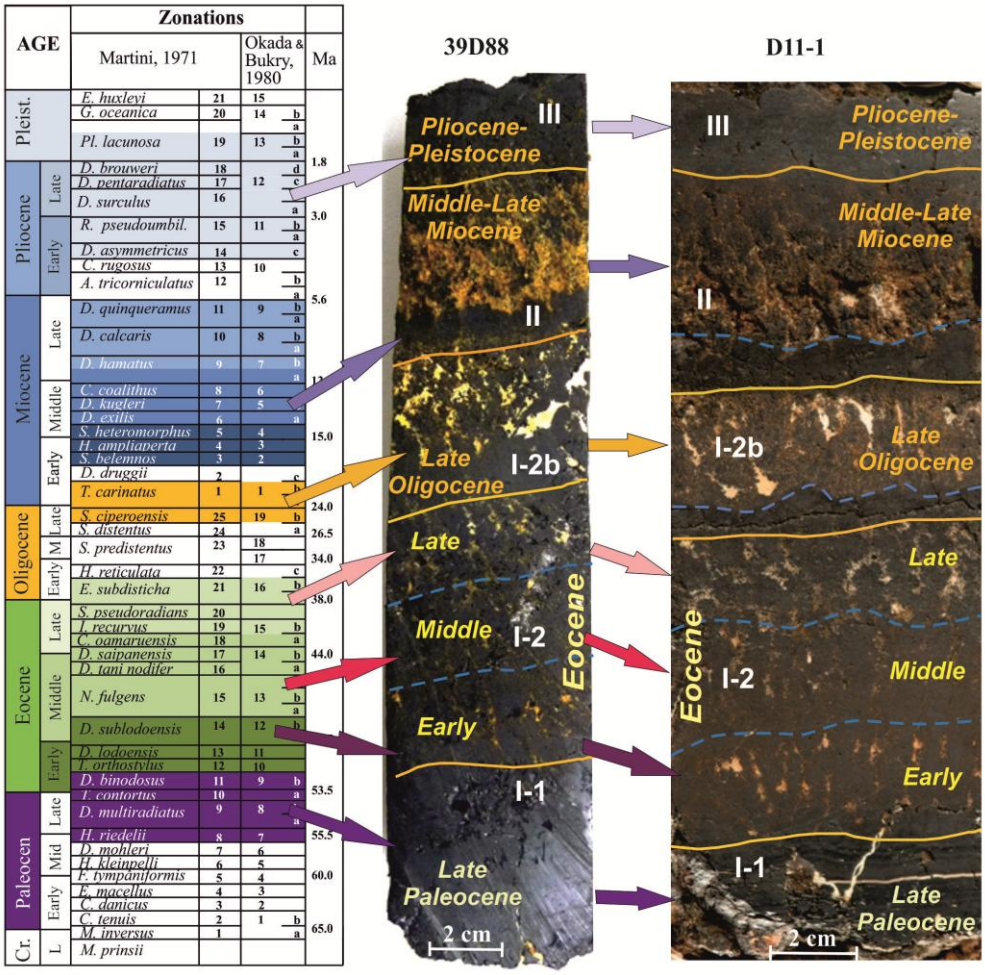

Figure 3. Cross sections of Fe-Mn crusts from Butakov and Lomilik guyots, with identified index species of calcareous nannoplankton [39–42] modified after a conference presentation [29].

1.3. Geochemistry of Minor and Trace Element of Hydrogenetic Fe-Mn Crusts: Main Features

The most often invoked model explains the formation of Fe-Mn crusts by precipitation of Fe and Mn oxyhydroxides incorporating Co, Ni, Cu, Mo, W, REE, Y, and other elements directly from seawater [1–11,33]. The distribution of Mn and Fe in seawater is controlled by its major-ion chemistry, pH, and contents of dissolved oxygen, organic matter, and carbon dioxide. Phytoplankton and skeletal organic material accumulate Co, Mn, Ni, and other metals till depths of 500 m [4,43]. The consumption of oxygen by organic matter produces an oxygen minimum zone (OMZ) at bathymetric levels of 500–800 m, below which the concentration of dissolved oxygen gradually increases. Decomposition of organic matter in the OMZ sub-reducing environment elevates dissolved Mn, whereas the greater depths beneath the OMZ provide favorable conditions for precipitation of Fe and Mn oxyhydroxides onto exposed rock surfaces of seamounts [43–45]. Mn phases interacting with bottom waters sorb positively charged dissolved metals and complexes, whereas negatively and/or zero charged ions are sorbed onto Fe phases [6,46]. Comparison of trace element patterns of different phases in hydrogenetic Co-rich Fe–Mn crusts from the central Pacific and Atlantic regions shows that Co, Ni, Zn, Ba, Li, and Tl are mainly sequestered by the Mn component, while the Fe component accumulates Cu, Pb, Hg, Be, Sc, Ti, Zr, Hf, Nb, Ta, Bi, In, Sn, Te, Th, Cr, As, Se, Mo, and W; the residual

 doi:10.20944/preprints202510.1578.v1

aluminosilicate component in phosphatized layers containing abundant CFA is enriched in Y, Bi, Pb, and Se [46].

Much of the previous work on the Co-rich Fe-Mn crusts focused on their bulk chemistry, especially the patterns of main valuable metals (Mn, Fe, Co, Ni, Cu) and associated trace elements. The geochemistry of crusts as a whole is controlled by the relative contributions of the constituent layers that contain, in varying proportions, Fe and Mn oxyhydroxides (Fe-vernadite, feroxyhyte, etc.), CFA, aluminosilicates, and a residual biogenic carbonate phase. The Fe-Mn ore matrix and accessory phases partition elements selectively [33,46]: Fe and Mn oxyhydroxides sequester REEs, Y, Cu, Zn, and V; Fe-vernadite accumulates Co, Zn, Ni, Mg, Ba, and Tl; feroxyhyte hosts As, Bi, Cu, Cr, Mo, Nb, Pb, Te, Ti, Th, W, and Zr; aluminosilicates bear Si, Al, K, Ti, Cr, Mg, Fe, Na, Sc, and Rb; CFA is a carrier of P, Ca, CO_2, Sr, and Y; and biogenic carbonate contains Ba, Sr, Ce, Cu, V, Ca, and Mg. The most comprehensive datasets on the chemical compositions of Fe-Mn crusts and nodules from different oceanic regions were presented in [3–5,44]. They include mean concentrations of major and trace elements and metals in hydrogenetic Co-rich Fe-Mn crusts from three Pacific regions (North Pacific Prime Zone, including the Magellan Seamounts, Non-Prime North Pacific, and South Pacific) determined from sets of 70 to 362 analyses [5,44].

The concentrations of trace elements in the bulk samples of MST Fe-Mn crusts estimated previously by the team of JSC *Yuzhmorgeologiya* [22] are: <1 ppm for Ta, Cs, Ag, Pt; 1–10 ppm for ∑REE, Rb, Be, Sc, Se, Cd, Sn, Hf; 10–100 ppm for LREE, Nb, Sb, W, U, Th, Cr, Ga, Te, Bi; 100–1000 ppm for Ce, La, Nd, Y, Zn, Mo, Zr, As, Tl; and >1000 ppm for Ce, Pb, Sr, and Ba. Other data represent the average bulk composition of Fe-Mn crusts [47]: the mean contents of Mn, Fe, Co, Ni, Cu, REE, and Y in crusts from Govorov, Il'ichev, Kocebu, Pegas, Alba, Pallada, Fedorov, Gramberg, Ita Mai Tai, Gelendzhik, and Butakov guyots, as well as the mean contents of Fe, Mn, Co, Ni, Cu, P_2O_5, Mo, TiO_2, Zn, Cu, REE, and Y in layers I-1, I-2, II, and III of the crusts.

The Fe-Mn crusts from Pallada, Gramberg, Ita Mai Tai, Gelendzhik, and Butakov guyots were reported to share some geochemical features [22]. The relict layer R is highly heterogeneous due to abundant carbonate-phosphate material and often shows abnormally high Cu, Ni, Ba, Sr, Cr, Sc, Li, Zn, Hf, and Th concentrations. Layer I has the highest enrichment in Ce, Pb, Sr, Ba, Mo, Te, and Bi, as well as La, Zn, and Th on some guyots. Layer I-2 has the lowest overall trace element contents but is characterized by high Y, Cr, Sc, and Zr. The trace element distribution in Layer II is poorly consistent, with elevated Rb, Cs, Li, Zr, Sb, Nb, and Zn but low Sr and Bi. Layer III is enriched in As, Tl, and W while being depleted in Ba and Zn.

The geochemistry and mineralogy of separate layers of the crusts sampled on Ita Mai Tai, Gelendzhik [48,49], Govorov, Vulkanolog, Kocebu [50–52], Gordin, Pegas [53], Pallada [54,55], and Shkolnik [56] guyots have been studied in more or less detail.

In this review we synthesize dispersed data on the geochemistry and chronostratigraphy of MST Co-rich Fe-Mn crusts. The compositions of several crust samples from Govorov and Kocebu guyots are detailed and compared with a crust sample from Pallada Guyot [55], as well as, analytical results from earlier publications and technical reports of JSC *Yuzhmorgeologiya* on contents of minor and trace elements in the MST crusts. The review addresses geochemical features, element correlations, Co-chronometry, growth rates, ages, and the history of crust layers precipitated on the MST guyots.

2. Geological Background of Govorov and Kocebu Guyots

Govorov Guyot is the largest in the MST, with its 190×180 km base lying along the 4700 m isobath, a trapezium-shaped main body with 70–90 km sides, and a 79×53 km flat top [12,18,19,50,51] (Figure 4a).

 doi:10.20944/preprints202510.1578.v1

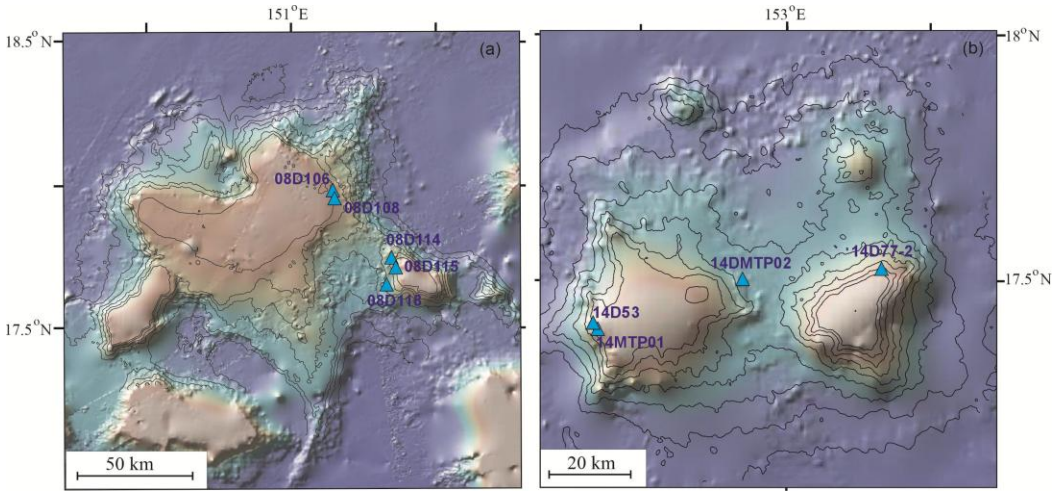

Figure 4. Bathymetry maps of Govorov (a) and Kocebu (b) guyots. Bold lines in panels (c) and (d) are isobaths at 500 m intervals. Triangles mark location of dredging sites.

The main edifice is extended with two satellites oriented in the southwestern and southeastern directions and large offshoots in the south and northeast. The slopes of the main edifice dip at 4–8° to 25°; the northern and northeast slopes are shallower (10–15°) than the western and eastern slopes until the 4500 m depth. The northeastern edge and flat top are delineated by a chain of volcanic cones up to 100 m high with 0.6–2.5 km base diameters [13]. The main guyot edifice and its satellites are composed mostly of volcanic rocks. The rocks exposed on slopes are fine to boulder-size lava and tuff clasts, hyaloclastics, pillow lavas, or lava flows with columnar jointing. Eroded volcanic and sedimentary rocks affected by seawater alteration are cemented with calcareous coccolith-foraminiferal material and form so-called edaphogenic breccias. The volcanic rocks reach thicknesses of ~1700–1800 m on the southwestern slope and up to 2900 m on the northeastern slope. The summit platform and low-angle slopes of the guyot are locally covered by Aptian to Pliocene carbonate sediments [9,12,19]. The surfaces swept from unconsolidated sediments, mainly along the top edge to sea depths of 2200–2400 m, are paved with Co-rich Fe-Mn crusts, from 0.7 to 14.5 cm thick, with occasional occurrences of Fe-Mn nodules.

Kocebu Guyot consists of two (western and eastern) flat-topped edifices of 115×95 km and ~10000 km² total size (Figure 4b). The two summit platforms are separated by a saddle at 3500–3700 m below the sealevel, while the pedestals of the main edifices reach water depths of 5100–5500 m [9,12,52]. The eastern edifice sits upon a 42×41 km (~ 1000 km²) triangular base and has a 20×16.5 km (~180 km²) summit platform 1200–1400 m under the water. The western edifice is larger (55×52 km or ~1400 km²) and has several offshoots. Both edifices have convex-concave transversal profiles and steep slopes (20–25°) till water depths of 2300–3000 m. Volcanic eruptions produced more than 200 small cones and domes (0.5–1.5 km across and 50–100 m high) upon the slopes and offshoots of the guyot while carbonate deposition left remnants of a lagoonal coral reef with lenses of stratified sediments on the tops.

The Co-rich Fe-Mn crusts of Govorov and Kocebu guyots precipitated upon Late Cretaceous and Early Paleogene bioclastic limestones, edaphogenic breccias, volcanic, and volcaniclastic rocks. All crusts bear Fe-vernadite and Mn-feroxyhyte as main minerals in all layers. Layers I-1 and I-2, and less often layer II, contain asbolane-buserite and CFA. The distribution, textures, structures, and mineralogy of the Govorov and Kocebu Fe-Mn crusts (including those from dredging sites 08D106, 08D115, 14MTP01 and 14D77, Figure 4), were described in detail previously [50–52].

 doi:10.20944/preprints202510.1578.v1

3. Materials and Methods

3.1. Sampling

Cobalt-rich Fe-Mn crusts were retrieved by dredging and coring of shallow boreholes in the course of cruises by JSC *Yuzhmorgeologiya*. The most representative samples of crusts were separated from the volcanic, volcaniclastic, and sedimentary substrate, in bulky pieces of >10 kg. Samples of layers were cut out from the thickest crusts with a diamond saw. Note, however, that thus obtained samples may bear fragments of transition zones between layers rather than being representative of a single layer. The samples were kept in muffle furnaces at 105°C at least 24 hours and then crushed, quartered, and ground.

The Fe-Mn crusts used for this study were dredged from Govorov and Kocebu guyots during the cruises of R/V *Gelendzhik* (JSC *Yuzhmorgeologiya*) in 2016–2017 (Figure 4, coordinates of dredging sites and 30 crust layer sample numbers are provided in Table 1 for 9 crust sections). Samples of Govorov crusts were selected in the eastern part of the main edifice (08D106, 08D108), as well as on the summit plateau and slopes of its satellite southeast of the main edifice (08D115, 08D114), and 08D118-3. The Kocebu crusts were collected on the slopes of the western edifice (14D53, 14MTP01, 14MTP02) and near the edge of the eastern edifice (14D77-2).

Table 1. Location of dredging sites at Govorov and Kocebu guyots.

Sampling sites	Deposit Type (Crust layer samples)	Latitude (N)	Longitude (E)	Sea depth, m
Govorov				
08D106	Crust (I-1, I-2, II-1, II-2, III)	17°55.416'	151°14.111'	1780
08D108	Crust (II-1, II-2, III)	17°53.903'	151°14.488'	2037
08D115	Crust (I-1, II, III)	17°37.201'	151°29.888'	1900
08D114	Crust (I-1, II, III)	17°39.611'	151°28.809'	2249
08D118-3	Crust (I-1, II, III)	17°33.101'	151°27.571'	2832
Kocebu				
14D53	Crust (I-2, II, III)	17°22.431'	152°33.218'	1794
14MTP01	Crust (I-1)	17°22.346'	152°33.056'	1958
14MTP02	Crust (I-1, II, III)	17°27.555'	152°51.043'	2695
14D77-2	Crust (I-1, I-2, II-1, II-2, III)	17°29.877'	153°13.693'	1538

Dredging was performed within a 600 m long interval; coordinates and sea depths are given for the starting point of dredging.

3.2. XRF and ICP-MS Chemistry of Fe-Mn Crusts

The samples of hydrogenetic Co-rich Fe-Mn crusts from Govorov and Kocebu guyots were analyzed for bulk chemistry at the Center for Isotope-Geochemical Studies of the Vinogradov Institute of Geochemistry, Siberian Branch of the Russian Academy of Sciences (IGC SB RAS, Irkutsk) by several methods: XRF on a Bruker AXS S4 Pioneer wavelength dispersive X-ray fluorescence spectrometer using glass fusion discs (for SiO_2, TiO_2, MgO, Fe_2O_3 tot, MnO tot, CaO, K_2O, Na_2O, P_2O_5, LOI, Ba, Sr, Zr, V, Co, Ni, Cu, and Zn). Minor and trace elements (Co, Ni, V, Cu, Sb, W, Mo, Zn, Be, Rb, Ba, Th, U, Nb, Ta, Pb, Ga, As, REE and Y) were determined by mass spectrometry with inductively coupled plasma (ICP-MS) after acid digestion of samples, on an Agilent NexION 300D quadrupole mass spectrometer. The quality of XRF and ICP-MS analyses was checked against local standards CDO-4, CDO-5, CDO-6 [57] and USGS international standard AGV-2.

The data were processed statistically using the *Statistica 10* software (StatSoft). The correlation coefficients were used to calculate matrices for the chemical data to measure the strength of linear relationship between pairs of variables. Statistical significance is quoted at the 95% confidence level. Element relationships were constrained by factor analysis of principal components (varimax raw) to identify groups of major and trace elements. REE and Y plots were normalized to the respective

 doi:10.20944/preprints202510.1578.v1

contents in the Post-Archean Australian Shale (PAAS) [58]. The Ce anomaly was calculated as Ce* = 2Ce/(La + Pr) for PAAS-normalized values.

4. Results

The XRF data revealed major and minor element patterns of Co-rich Fe-Mn crusts from nine sampled sections in Govorov and Kocebu guyots (Figure 5, Tables A1 and A2 in Appendix A), which were compared with data on a crust from Pallada Guyot [55].

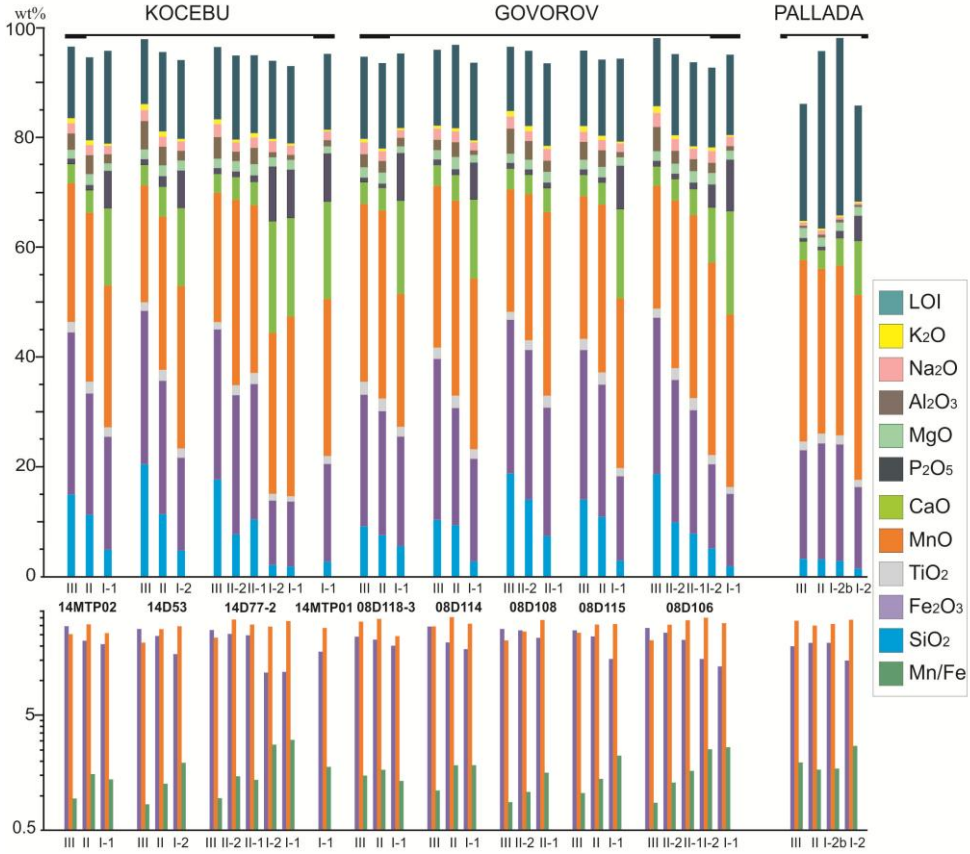

Figure 5. Summary of XRF data for layers of crusts from Kocebu and Govorov guyots (Tables A1 and A2 in Appendix A), as well as layers of the crust (from EPMA and XRF data) from Pallada Guyot, after [55]).

Samples from all layers show relatively high LOI of 12-15 wt.% (presumably due to atmospheric moisture adsorbed on the ground ore material) and quite large ranges of major oxides: 12-29 wt% Fe_2O_3 tot, 22-35 wt% MnO tot, 3.4-20 wt% CaO, 1-9.4 wt% P_2O_5, at modest amounts of TiO_2 (1-2 wt%), MgO (1.3-2 wt%), Na_2O (1.6-2.5 wt%), and K_2O (0.3-1.2 wt%). The highest concentrations of Ca and P were measured in phosphatized layers (I-1 and I-2). The excess of Fe over Mn increases from layer I-1 to layer III, while the Mn/Fe ratio decreases from 3-2.5 to 1.5-0.8. Layers II and III in all crusts show SiO_2 and Al_2O_3 enrichment due to the presence of silicate phases (quartz, feldspars, etc.). The crust from Pallada Guyot contains 1.5-3.2 wt% SiO_2 and displays minor variations of the Mn/Fe ratio (1.7-1.9) in the average compositions of layers I-2, I-2b, II and III (Figure 5).

4.1. Contributions of Layers to the Bulk Composition

Evaluating the mineral potential of Co-rich Fe-Mn crusts and their viability as commercial resources of metals requires data on chemistry of the crusts as a whole and their individual layers. Sampling during the cruises of JSC *Yuzhmorgeologiya* commonly includes several procedures: measuring the average thicknesses of crusts and their layers, estimating physical parameters (density, moisture content, porosity, etc.), and analyzing major, minor and trace elements in bulk crust or less

 doi:10.20944/preprints202510.1578.v1

often layer samples. The contribution (weigth fractions, wt%) of layers to the bulk crust composition is hard to estimate from their linear sizes. Such calculations are made with regard to the density of layers varying from ~2.1 g/cm^3 in Layer I-1 to ~1.9 g/cm^3 in Layer III [9] and can yield only approximate estimates because the crusts have complex cross-sectional structure even within single large samples (Figure 6). The problem was solved using mass-balance calculations of major oxide contents (Table 2), for each layer relative to the bulk composition of crusts from Govorov (08D106, 08D115) and Kocebu (14D77-2, 14D53) guyots and statistical data.

Table 2. Contributions of layers (weight fraction) to the bulk Fe-Mn crusts composition.

	08D106	**ΔX**	**Layer**	**wt%**		**08D115**	**ΔX**	**Layer**	**wt%**
SiO_2	13.10	0.082	III	47.02	SiO_2	9.95	0.176	III	53.13
TiO_2	1.99	0.098	II-2	21.93	TiO_2	1.85	-0.001	II	13.45
Al_2O_3	3.08	-0.122	II-1	18.41	Al_2O_3	2.13	-0.272	I-1	29.16
Fe_2O_3	25.00	-0.118	I-2	12.25	Fe_2O_3	22.20	0.003	Total	95.73
MgO	2.05	0.178	I-1	0.04	MgO	1.87	0.208		
MnO	27.42	-0.205	Total	99.64	MnO	26.94	0.033		
CaO	4.49	-0.114			CaO	7.03	-0.296		
Na_2O	2.48	0.209			Na_2O	2.36			
K_2O	0.82	-0.075			K_2O	0.71	-0.034		
P_2O_5	1.52	0.065			P_2O_5	3.14	0.184		
LOI	15.40				LOI	15.84			
Total	97.35				Total	94.03			
$\sum\Delta X^2$		0.185			$\sum\Delta X^2$		0.271		
	14D77-2	**ΔX**	**Layer**	**wt%**		**14D53**	**ΔX**	**Layer**	**wt%**
SiO_2	10.13	0.197	III	27.98	SiO_2	11.38	0.229	III	2.35
TiO_2	1.73	0.101	II-2	28.99	TiO_2	1.82	-0.146	II	94.10
Al_2O_3	2.21	-0.237	II-1	22.32	Al_2O_3	2.94	-0.371	I-2	0.00
Fe_2O_3	22.80	-0.192	I-2	13.24	Fe_2O_3	23.33	-0.231	Total	96.45
MgO	2.06		I-1	7.89	MgO	2.02	0.115		
MnO	29.73	0.090	Total	100.42	MnO	27.00	0.272		
CaO	6.96	-0.233			CaO	4.74	-0.457		
Na_2O	2.46				Na_2O	2.39			
K_2O	0.76	0.112			K_2O	0.80			
P_2O_5	3.05	0.163			P_2O_5	1.43	-0.420		
LOI	16.35				LOI	16.57			
Total	98.23				Total	94.40			
$\sum\Delta X^2$		0.243			$\sum\Delta X^2$		0.739		

Note. ΔX is the difference between the initial and calculated oxide contents.

The calculations were performed with the minimum values of the statistical parameter $\sum\Delta X^2$ (sum of square residuals of the initial and calculated oxide contents using the least squares method) for different sets of major oxides (SiO_2, TiO_2, Al_2O_3, Fe_2O_3, MgO, MnO, CaO, Na_2O, K_2O, and P_2O_5, Tables A1 and A2 in Appendix A). The mass-balance estimates showed that Layer III contributed 47 and 53 wt% into the bulk crust composition of samples 08D106 and 08D115, respectively, at $\sum\Delta X^2$ = 0.19 and 0.27 (Table 2). These contributions are 2.3 and 1.3 times higher than the estimates based on the average thickness of layer III: 20% for 08D106 and 42% for 08D115. The large discrepancy may

 doi:10.20944/preprints202510.1578.v1

result from variability of layer thicknesses, as in samples 08D106 and 14D77-2 (Figure 6). Note also that the layer compositions can be estimated from small crust fragments selected in laboratory, which allows relating metals to specific layers more precisely.

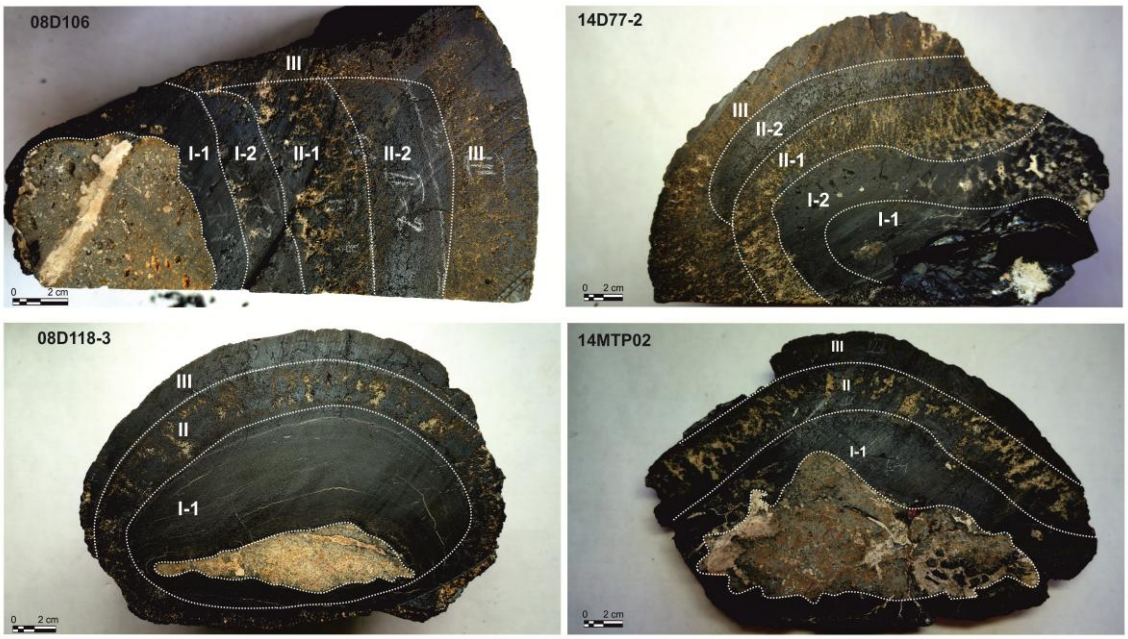

Figure 6. Sections of Co-rich Fe-Mn crusts sampled from Govorov (08D106, 08D118-3) and Kocebu (14D77-2, 14MTP02) guyots.

4.2. Minor and Trace Element Chemistry

4.2.1. High-Tech Metals (Co, Ni and Cu), Ba, Sr, Pb, Zn, V, Mo, Zr, Nb, W, Sb, and As

The concentrations of Co and Ni vary from 4000 to 7200 ppm and from 3000 to 8700 ppm, respectively, across the crusts from Kocebu, Govorov and Pallada guyots (Figure 7; Tables A3 and A4 in Appendix A). There is no evident correlation between the two elements: the amount of Co is the highest (8694 ppm) in Layer III from sample 08D118-3 but is the lowest (as well as Ni) in the same layer of other crust samples where it mostly occurs in Layers II or I-2. The crust from Pallada Guyot contains the lowest amount of Co and Ni in Layers I-2b and II, while Layers I-2 and III show the greatest enrichment in both elements. The Cu contents range from 700 to 2500 ppm being the highest in Layer II and lower in Layer III of the Govorov and Kocebu samples, and decrease progressively in the series I-2 → I-2b → II → III in the crust from Pallada Guyot. In all sections, Layer I-1 typically shows the highest enrichment in Ba and Sr and sometimes in Zn and Mo. Layer III bears As in most of the samples while Layer II (II-1 and II-2) is enriched in Zr, Nb, and Sb, and occasionally W.

 doi:10.20944/preprints202510.1578.v1

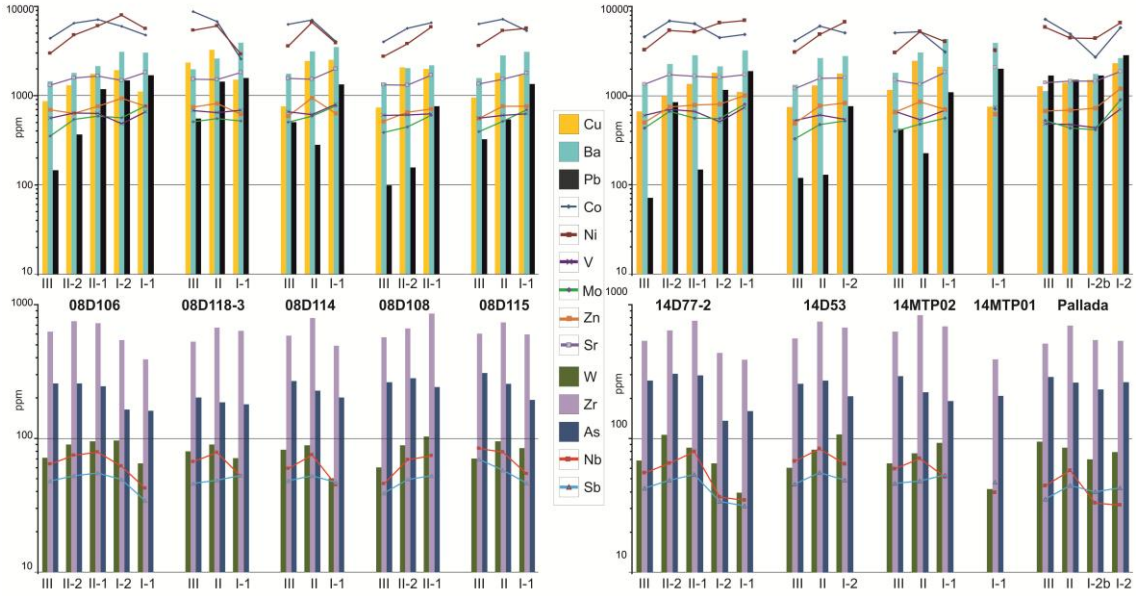

Figure 7. Patterns of trace elements (ppm) in different layers of crusts from Govorov and Kocebu guyots, this study (Tables A3 and A4 in Appendix A), and in crust from Pallada Guyot, after [52].

4.2.2. REE and Y

The abundances of REE and Y in the Co-rich Fe-Mn crusts from Kocebu and Govorov guyots vary in large ranges and show consistent variations in separate layers (Figures 8 and 9; Tables A3 and A4 in Appendix A). The sum REE and Y decreases from 3546–2360 ppm in Layers I-1 and I-2 to 2188–1312 ppm in II, while Ce accounts for <60% of this sum. Cerium is especially high in Layer I-1 (1354 ppm to 2177 ppm in samples 14D77-2 and 14MTP01, respectively) where it contributes 50–61% to REE+Y, but its concentration and contribution in Layer III are much lower: 535–612 ppm and 48-38%, respectively. The abundances of Y, La, and Gd likewise decrease from I-1 to III but less markedly than for Ce (Figure 8).

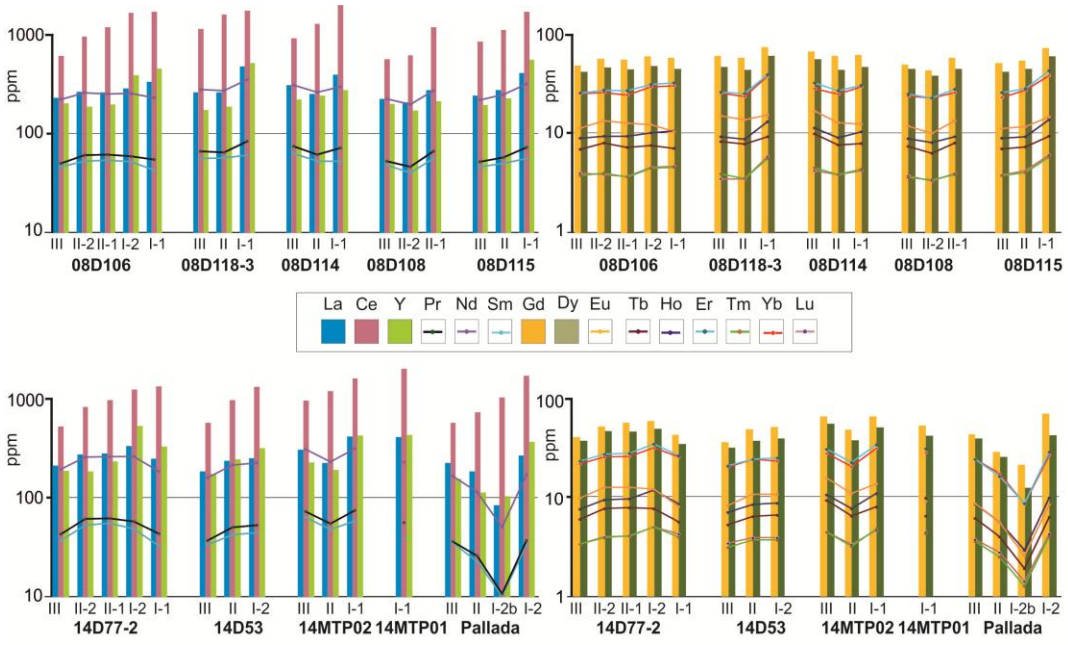

Figure 8. REE and Y patterns (ppm) in different layers of Co-rich Fe-Mn crusts from Govorov and Kocebu guyots, this study (Tables A3, A4 in Appendix A), and Pallada Guyot, after [55].

 doi:10.20944/preprints202510.1578.v1

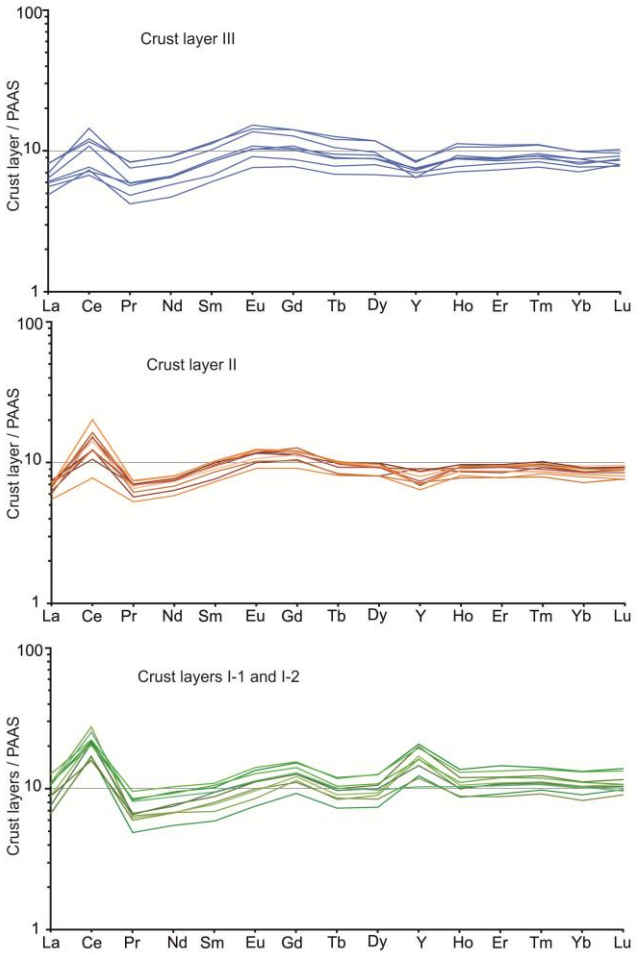

Figure 9. PAAS-normalized REE and Y patterns in different layers of Co-rich Fe-Mn crusts from Govorov and Kocebu guyots.

Other REEs (Pr, Nd, Sm, Eu, Tb, Dy, Ho, Er, Tm, Yb, and Lu) have irregular patterns, either decreasing (08D115, 08D106, 08D118-3, 14D77-2, 14D53) or increasing (08D114, 14MTP02) within small intervals. The crust from Pallada Guyot shows a decreasing trend of Ce and REE+Y from early to younger layers, while other REEs and Y become progressively higher in the series I-2b → II → III (Figure 8).

The PAAS-normalized REE+Y patterns of crusts from Govorov and Kocebu guyots are marked by a positive Ce anomaly, with its magnitude (Ce^*) decreasing gradually toward younger layers (Figure 9; Tables A3 and A4 in Appendix A). The Y anomaly is positive in Layers I-1 and I-2 but negative in II and III.

5. Discussion

5.1. Average Chemistry of Bulk Crusts and Individual Layers

The bulk chemistry of Co-rich Fe-Mn crusts from the MST guyots was characterized using 309 to 803 XRF, mass spectrometry, and ICP-MS analyzes obtained before 2009 [47], as well as statistical data (mean, median, minimum and maximum values and variance) for 276 ICP-MS analyses for minor and trace elements complied from technical reports of JSC *Yuzhmorgeologiya* before 2017 and our nonpublished data on Govorov and Kocebu guyots (Table A5 in Appendix A). The mean contents of elements estimated by different methods and in different time intervals are generally consistent, with discrepancy of < 20–25%. The concentrations of main valuable elements vary in large ranges (percentages in brackets are variance): 2700–9000 ppm Co (19%), 1200–6700 ppm Ni (19%), 520–2113

 doi:10.20944/preprints202510.1578.v1

ppm Cu (21%), 140–600 ppm Mo (19%), 320–801 ppm Zn (19%), 352–1700 ppm Pb (21%), 92–260 ppm As (17%), and 1006–3228 ppm REE+Y (21%). Most of elements show quasi-normal distribution patterns at variance from 9 to 40%. The concentrations of Cr, Li, Be, Cs, Ta, Zr, and Hf have the highest variance and lognormal distribution. The discrepancy between the mean and median values is the most prominent for Cr (16.5 and 11 ppm, 277%), Zr (231 and 120 ppm, 106%) and Hf (3 and 1.8 ppm, 94%) (Table A5 in Appendix A).

The chemistry of crusts as a whole depends on the contributions (weight fractions) of the constituent layers (Table 2) which may have different geochemical characteristics. This inference agrees with poor correlations among elements revealed by the factor analysis of principal components (varimax raw) for 276 ICP-MS analyses. Only REE and several pairs of trace elements have high correlation coefficients with $r > 0.7$ at 95% confidence level: Zr–Hf ($r = 0.92$), Zr–Ta ($r = 0.78$), Rb–Cs ($r = 0.78$), Zn–Sr ($r = 0.77$), Sb–Sn ($r = 0.73$), Nb–Sb ($r = 0.72$), and W–Tl ($r = 0.72$) (Supplementary Table S1). The correlation between these elements is obviously independent of the relative contributions of layer compositions to the whole-crust chemistry.

The data used to characterize the minor- and trace element compositions of the Fe-Mn crusts in this study included 118 ICP-MS analyses for Layers III, II, I-2, and I-1 in the crusts from Govorov and Kocebu guyots (Tables A3 and A4 in Appendix A) complemented with analyses from earlier publications [47,48,50–52] and technical reports of JSC *Yuzhmorgeologiya*. The data were processed statistically to estimate mean concentrations and variance for major elements and mean, median, maximum, minimum, and variance values for minor and trace elements (Tables A6 and A7, Appendix A). High variance (>50 %) at nearly lognormal distribution was observed for Cr, Li, Cs, Rb, Ta, Pb, Zr, Hf and Ga in Layer III (31 analyses); Cr, Li, Be, Cs, Rb, Ta, Zr, Hf and Ga in Layer II (33 analyses); Cr, Sb, Cs, Rb, Th, Nb, Ta, Zr and Hf in Layer I-2 (25 analyses); Cr, Sc, Li, Be, Rb, Cs, Ta, Zr and Hf in Layer I-1 (29 analyses). The mean ratio Mn/Fe decreases slightly from 1.85-1.68 in the old unit (Layers I-1, I-2) to 1.35-1.34 in the younger units (II, III). Layers I-1 and I-2 contain the highest concentrations of P but are depleted in Ti. The values of mean, median, maximum and minimum contents, REE+Y, L/HREE, and positive Ce anomaly (Ce*) vary markedly from layer to layer.

The variations of mean REE, Y, minor and trace elements in separate layers of the analyzed Fe-Mn crusts were plotted in a diagram of element contents normalized to the average composition of crusts from the Non-Prime North Pacific Zone, N-PNPZ [5,44]. Layers I-1 and I-2 are enriched in Ba, Sr, Pb, Mo, Bi, Te and depleted in Co, Cr, Sb, W, Li, Cs, Zr, Hf, Ga, As and Cd (Figure 10a,b), while Layer II stores the highest concentrations of Ni, Cu, Sn, Sb, W, Tl, Li, Cs, Rb, Nb, Zr, and Hf. Layer III contains more As, Ni, Ga and less Cu, Zn, and Te compared to other layers. The contents of Y are the highest in Layers I-1 and I-2, while Ce is the highest in Layer I-1 and the lowest in Layer III. Layer I-2 is depleted in Pr, Nd, Sm and Eu, while Layer II shows the lowest total of Ho, Er, Tm, Yb and Lu REEs.

The PAAS-normalized REE and Y patterns of separate layers are typical of hydrogenetic crusts, with a positive Ce anomaly (Ce*) decreasing from I-1 to III (Figure 10c).

 doi:10.20944/preprints202510.1578.v1

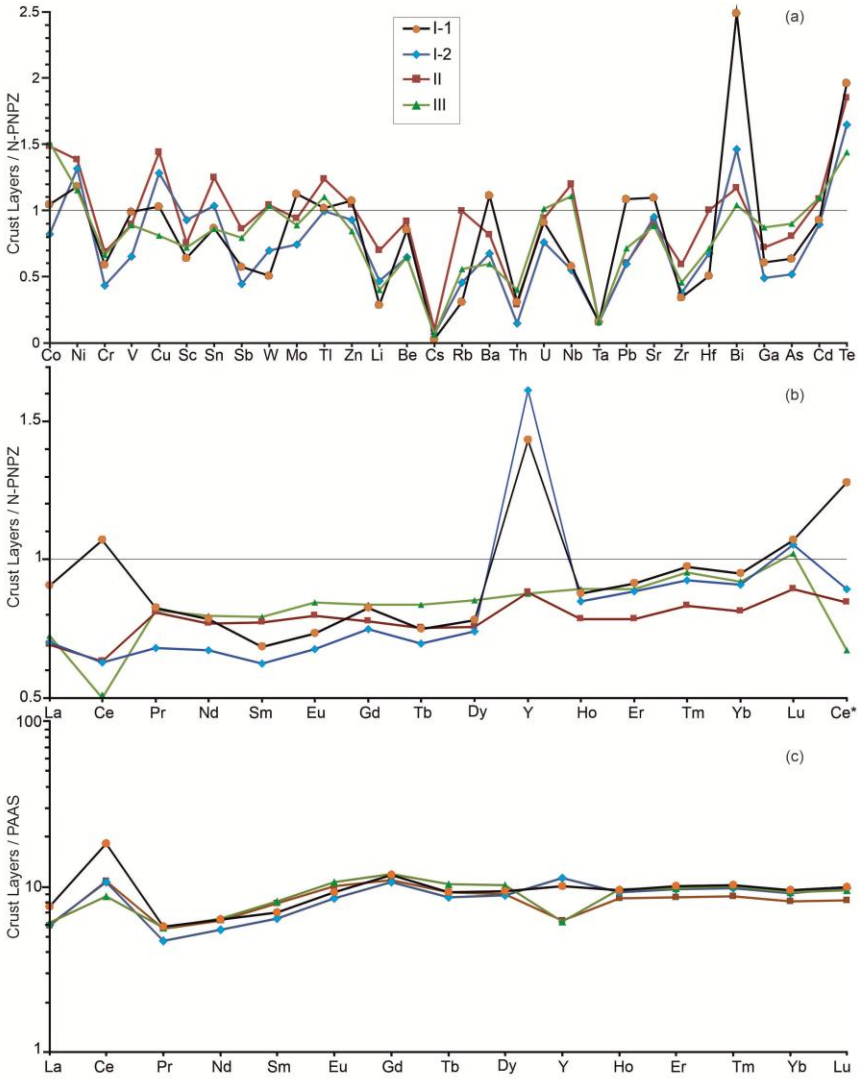

Figure 10. Mean contents of minor, trace elements, REE, Y, and Ce* normalized to N-PNPZ (Non-Prime North Pacific Zone, after [5,44] (a), (b), and PAAS, after [58] (c).

The (Ni+Co+Cu)–Mn–Fe and (Zr+Y+Ce)–(Fe+Mn)/4–(Co+Ni)×15 and Ce*–(Y/Ho)sn diagrams used for classification of Fe-Mn crusts confirm the hydrogenetic origin of the analyzed layers (Figure 11a,b). The phosphatized layers (I-1, I-2) are enriched in Y and plot isolated fields in the Ce*–(Y/Ho)sn and Ce*–Nd diagrams (Figure 11c,d).

 doi:10.20944/preprints202510.1578.v1

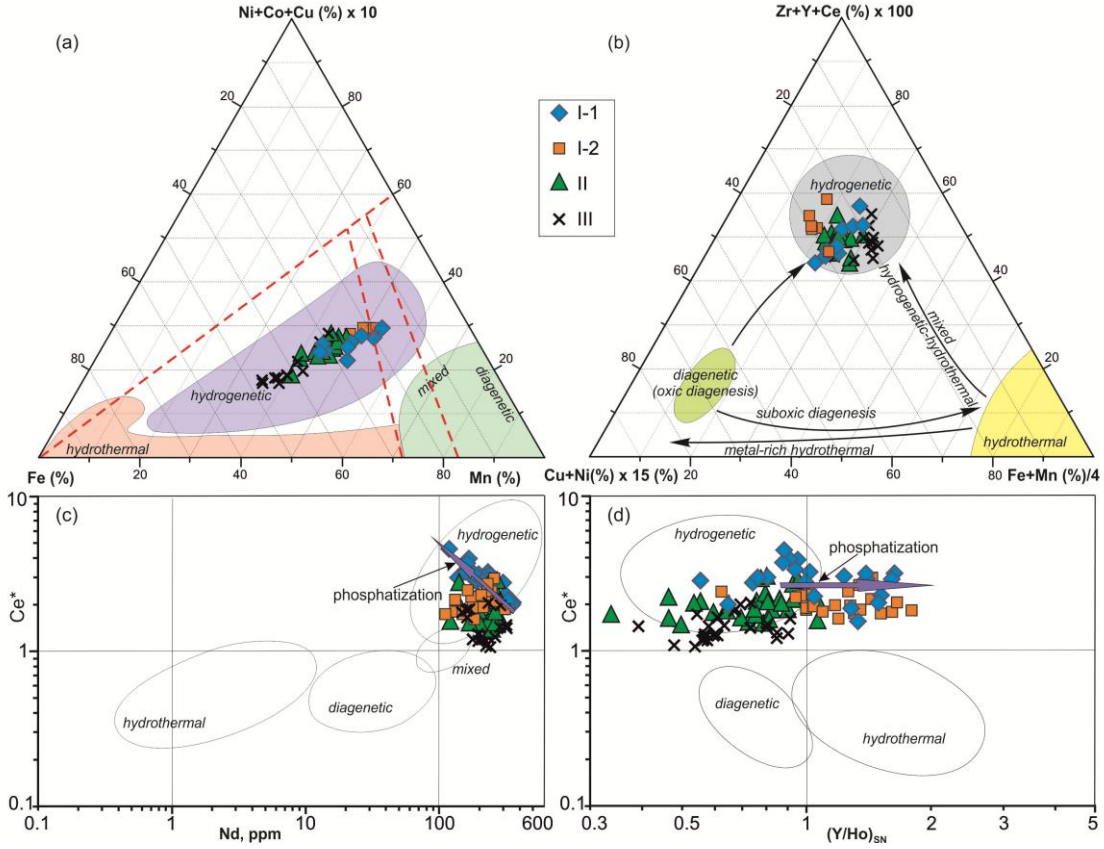

Figure 11. Ternary discrimination diagrams for Fe-Mn crusts and nodules: (Ni+Co+Cu)–Mn–Fe, after [59,60] (a); (Zr+Y+Ce)–(Fe+Mn)/4–(Co+Ni)×15, after [61] (b); and classification diagrams based on REE and Y, modified after [62] (c) and (d).

The complex geochemical characteristics of crust layers were grouped using the factor analysis of principal components (varimax raw) applied to a statistical sample of 118 analyses for 34 elements (Co, Ni, Cu, Sb, W, Mo, Zn, Be, Rb, Ba, Sr, Th, U, Nb, Pb, Zr, Hf, Ga, As, REE and Y), as well as the values of Ce*, the sums of LREE, HREE, REE+Y and the L/HREE ratio. The concentrations of Cr, V, Sc, Sn, Tl, Li, Bi, Cd and Te were not included because they remain non determined in many analyses. The strongest factor (1) which accounts for 34.7 % of total variance encompasses all REEs except Ce and La (Figure 12). Other second to fourth strongest factors with loadings >0.5-0.6 outline three more groups of elements: +(Ce, La, Ba, Mo, Sr, Pb), 16.6% of variance (factor 2); +(Zr, Hf, Nb, Rb, As)/-Pb, 13.9% of variance (factor 3), and +(U, Th, Co, As, Sb, W)/-Y, 7.5% of variance (factor 4).

According to factor 1 scores, the layers are compositionally similar, with close ranges of all REEs (Pr, Nd, Sm, Eu, Tb, Dy, Ho, Er, Tm, Yb, and Lu) except Ce and La. Factor 2 scores define the field of Layer I-1 with well pronounced correlations of Ce, Ce*, La, LREE, L/HREE, Ba, Mo, Sr, and Pb. Factor 3 corresponds to slightly elevated concentrations of Zr, Hf, Nb, Rb, As and high correlation between these elements in some compositions of Layers II and III. The lowest factor 4 scores are assigned to Layer I-2, with strong negative correlation between Y and the group U, Th, Co, As, Sb, W. Thus, the factor scores highlight composition fields, which are especially distinctive for Layers I-1, I-2 and II+III according to factors 2 and 4 (Figure 12).

 doi:10.20944/preprints202510.1578.v1

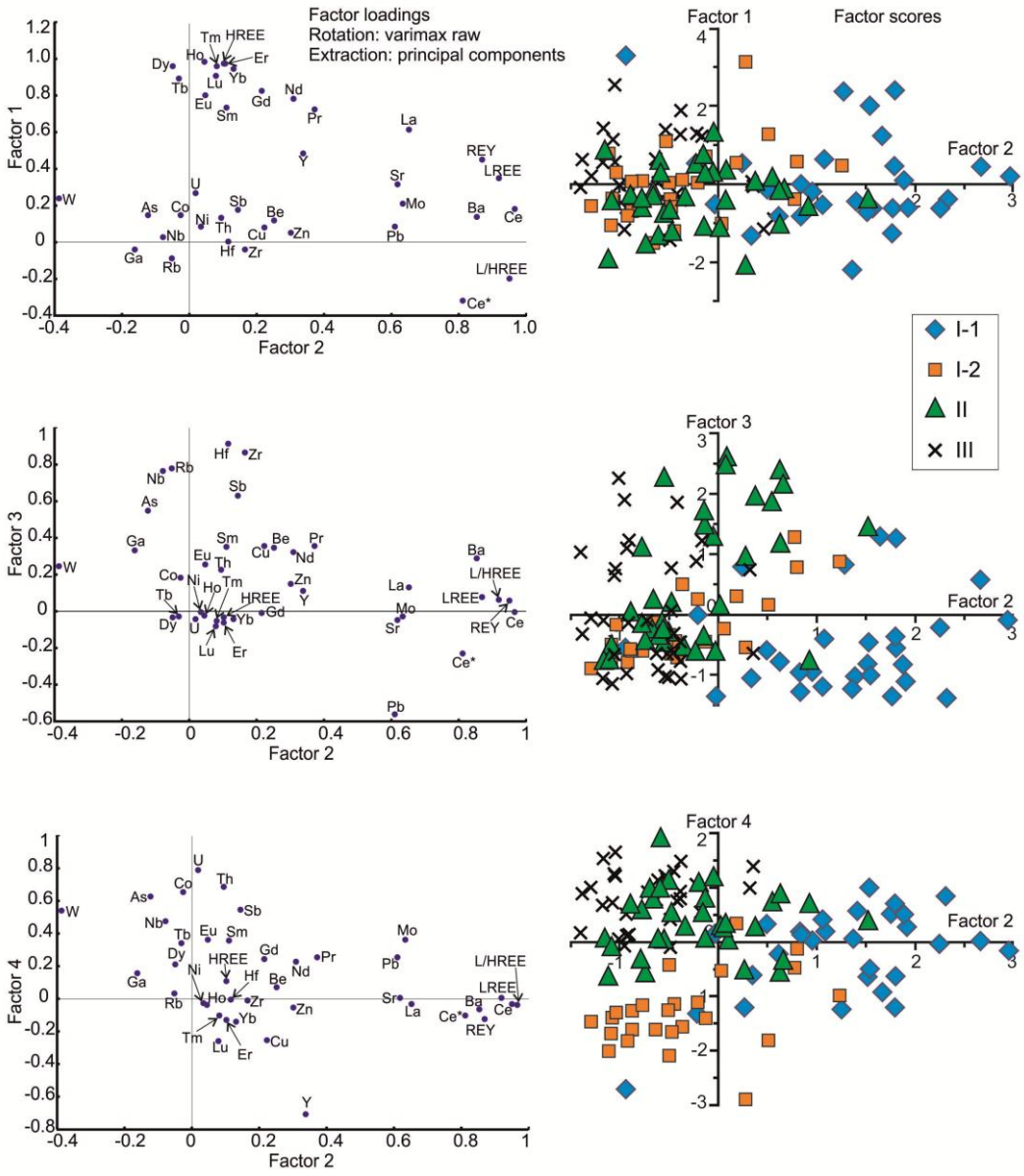

Figure 12. Grouping of elements by factor analysis of principal components (varimax raw) for layers in MST Fe-Mn crusts (see text for explanation). The plots show relationships based on factor loadings for elements and factor scores for layer compositions. .

5.2. Correlations Among Elements

Pairwise correlations of some elements and oxides demonstrate main features of difference between the old (I-1, I-2) and young (II, III) layers of the sampled Fe-Mn crusts (Figures 13–15). Correlation is the strongest in the pairs CaO and P_2O_5 (r = 0.99), Zr and Hf (r = 0.96), Rb and Cs (r = 0.97), and is quite high for Rb–Li (r = 0.84) and Li–Cs (r = 0.85), both in bulk crust compositions and in data for separate layers; most of REEs correlate at r = 0.6–0.8. Among other trace elements, only Ba, Nb, and Bi show high correlations (r ≥ 0.7) with Ce, La, LREE, REE+Y, Zr, Hf, and As: Ba–La (r = 0.84), Ba–LREE (r = 0.85), Ba-Ce (r = 0.73), Nb-Sb (r = 0.81), Nb–Hf (r = 0.73), Nb–Zr (r = 0.70); Nb–As (r = 0.67); Bi–Ce (r = 0.85), Bi–LREE (r = 0.80), and Bi–(REE+Y) (r = 0.80) (Supplementary Table S2).

 doi:10.20944/preprints202510.1578.v1

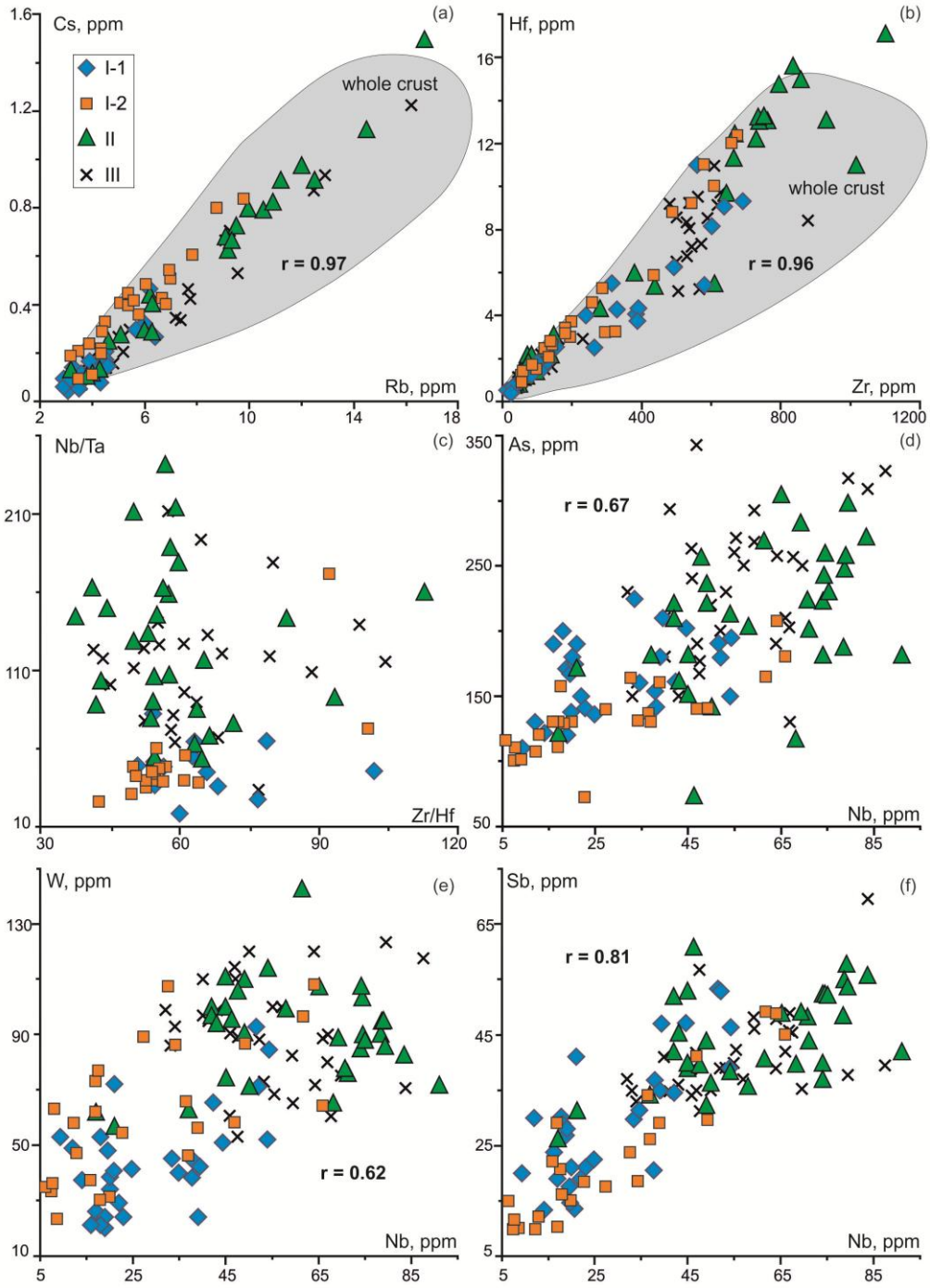

Figure 13. Concentrations of Nb, Zr, Hf, W, Sb, As and Zr/Hf and Nb/Ta ratios in layers of MST Fe-Mn crusts. Grey fields in panels (a) and (b) are bulk crust compositions.

The strongest correlation relationships for the compositions of crusts as a whole and their separate layers are detailed below.

 doi:10.20944/preprints202510.1578.v1

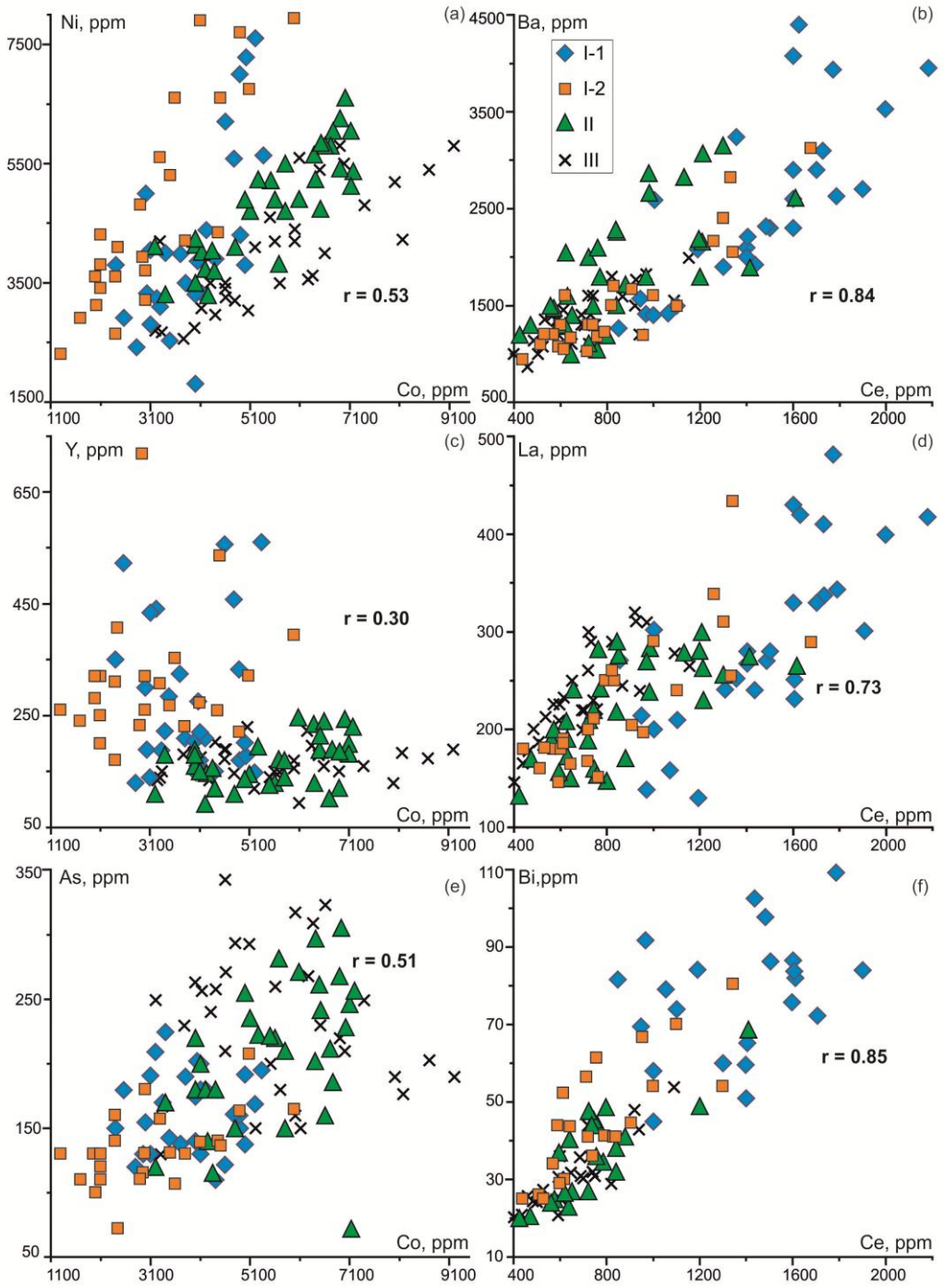

Figure 14. Concentrations of Co, Ni, Ce, La, Bi, and As in layers of MST Fe-Mn crusts.

5.2.1. CaO and P_2O_5

Variations of CaO and P_2O_5 were studied in Fe-Mn crusts from four guyots: Govorov and Kocebu, this study (Tables A1 and A2 in Appendix A), Ita Mai Tai [63] and Pallada [55]. The concentrations of CaO and P_2O_5 lack any significant correlation in Layers III and II which contain <4 wt% CaO and <1 wt% P_2O_5 (inset in Figure 15) but show almost perfect linear relationship in Layers I-2 and I-1, apparently due to the presence of carbonate fluorapatite (CFA). The highest possible CaO vs. P_2O_5 correlation (r ~ 1) is observed in all bulk crust, layer, and EPMA data for phosphatized samples (Figure 15).

The composition of CFA in phosphatized crusts from the Pacific Ocean is relatively uniform [64], with 30.15 wt% P_2O_5 and 53.17 wt% CaO on average (P_2O_5/CaO = 0.57). The average CFA composition

 doi:10.20944/preprints202510.1578.v1

was used to obtain empirical equations for estimating the wt% contents of CaO and CFA in crust samples where CaO > 4 wt% and P_2O_5 > 1 wt%: CaO = 2.3133 + 1.66867×P_2O_5 and CFA = 3.4305×(P_2O_5 – 1). The contents of CFA reach 50 wt% in the most phosphatized Layer I-2 in the crust from Kocebu Guyot (Figure 15).

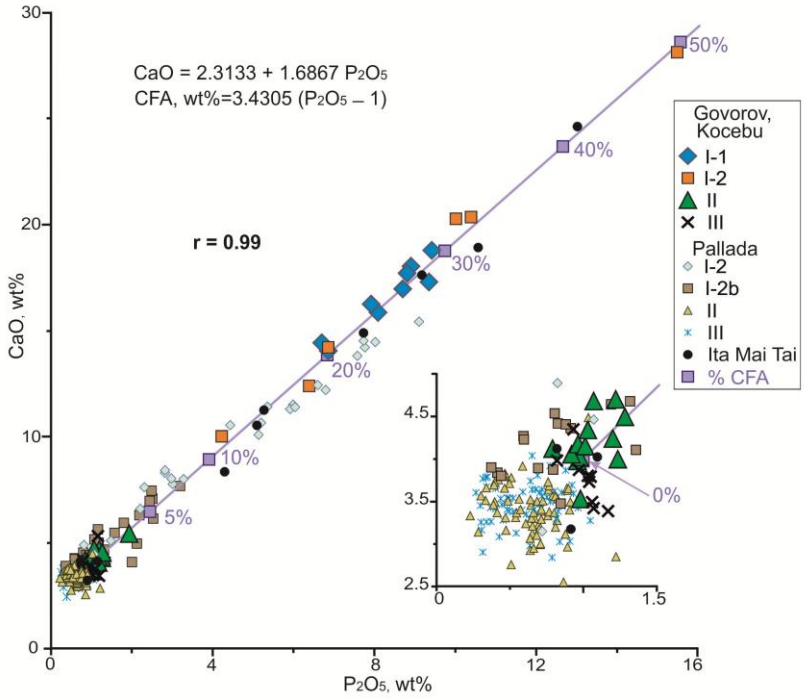

Figure 15. Variations of P_2O_5 and CaO in MST Fe-Mn crusts. See text for explanation.

5.2.2. High Field Strength Elements (Nb, Ta, Zr, Hf), Metalloids (Sb, As), W, and Alkali Metals (Rb, Cs, Li)

Correlation is the strongest (r = 0.92–0.96) between Zr and Hf in all bulk and layer compositions, but the distributions of the two elements differ in crust layers. Their concentrations vary in very large ranges both in crusts as a whole and in separate layers: from 15–22 ppm to 1100–1200 ppm Zr and 0.4–0.5 ppm to 17 ppm Hf (Figure 13b). The Zr and Hf enrichment is high in Layer II from most of the Govorov and Kocebu crust samples (Figure 7); some zones of high Zr (1100–1400 ppm) and Hf (20–35 ppm) also exist in Layer II of the crust from Pallada Guyot. The Zr/Hf ratio ranges from 32 to 259 over the whole crusts and from 31 to 184 within layers.

Niobium and tantalum correlate rather poorly in both bulk crust and layer compositions, at the concentration ranges of 7.6 ppm to 91 ppm (Nb) and 0.1 to 1.7 ppm (Ta). The Nb enrichment is higher in the young layers relative to the old units of the Fe-Mn crusts (Figure 13d–f), while the Ta variations are moderate. Correspondingly, the Nb/Ta ratio increases from 43–60 in Layers I-1 and I-2 to 60–240 in II and III (Figure 13c). The crust from Pallada Guyot shares similarity with the Govorov and Kocebu samples in the contents of Nb and Ta and in the patterns of Nb and Nb/Ta in the respective layers.

The concentrations of Sb, As, and W are commonly higher in younger layers (II, III) and correlate with Nb contents in the crusts from Govorov and Kocebu guyots (Figure 13d–f), but this trend is uncommon for the Pallada sample, where Sb enrichment is restricted to a few zones in Layer II.

Among alkali metals, only Rb concentrations reach high levels of 18–34 ppm and correlate at as high as r > 0.9 with Cs, in all bulk crust and layer compositions (Figure 13a). The crust from Pallada Guyot contains up to 230 ppm Rb, 28 ppm Cs, and 60 ppm Li in a single point from Layer III, which may be due to a K-feldspar grain that fell within the local spot of the LA-ICP-MS analysis.

 doi:10.20944/preprints202510.1578.v1

The iron and carbonate components of the hydrogenetic Fe-Mn crusts mainly sequester Rb and Cs [46], while Li, Zr, Hf, Nb, Ta, Sb and As are mostly incorporated into the iron component. These elements migrated into the crusts from seawater containing the $Zr(OH)_4^o$ > $Zr(OH)_4^-$, $Hf(OH)_4^o$ > $Hf(OH)_4^-$, $Nb(OH)_6^-$ > $Nb(OH)_5^o$, $Ta(OH)_6^-$ > $Ta(OH)_5^o$, and $HAsO_4^{2-}$ complexes.

5.2.3. REE, Y, Ba, Sr, and Bi

All PAAS-normalized REE patterns of hydrogenetic Fe-Mn crusts differ in a positive Ce anomaly and slight HREE enrichment over LREE (Figures 9 and 10c). The REE and Y patterns for MST crusts, including those from Govorov and Kocebu guyots, display decreasing Ce, Y, REE+Y, and Ce* trends from phosphatized old Layers I-1 and I-2 to younger Layers II and III, while the behavior of other REEs is less consistent (Figure 8). However, the REE and Y trends in the Pallada crust are more regular, especially upwards from Layers I-2b to III: Ce and Ce^* decrease while other REEs and Y increase gradually (Figure 16).

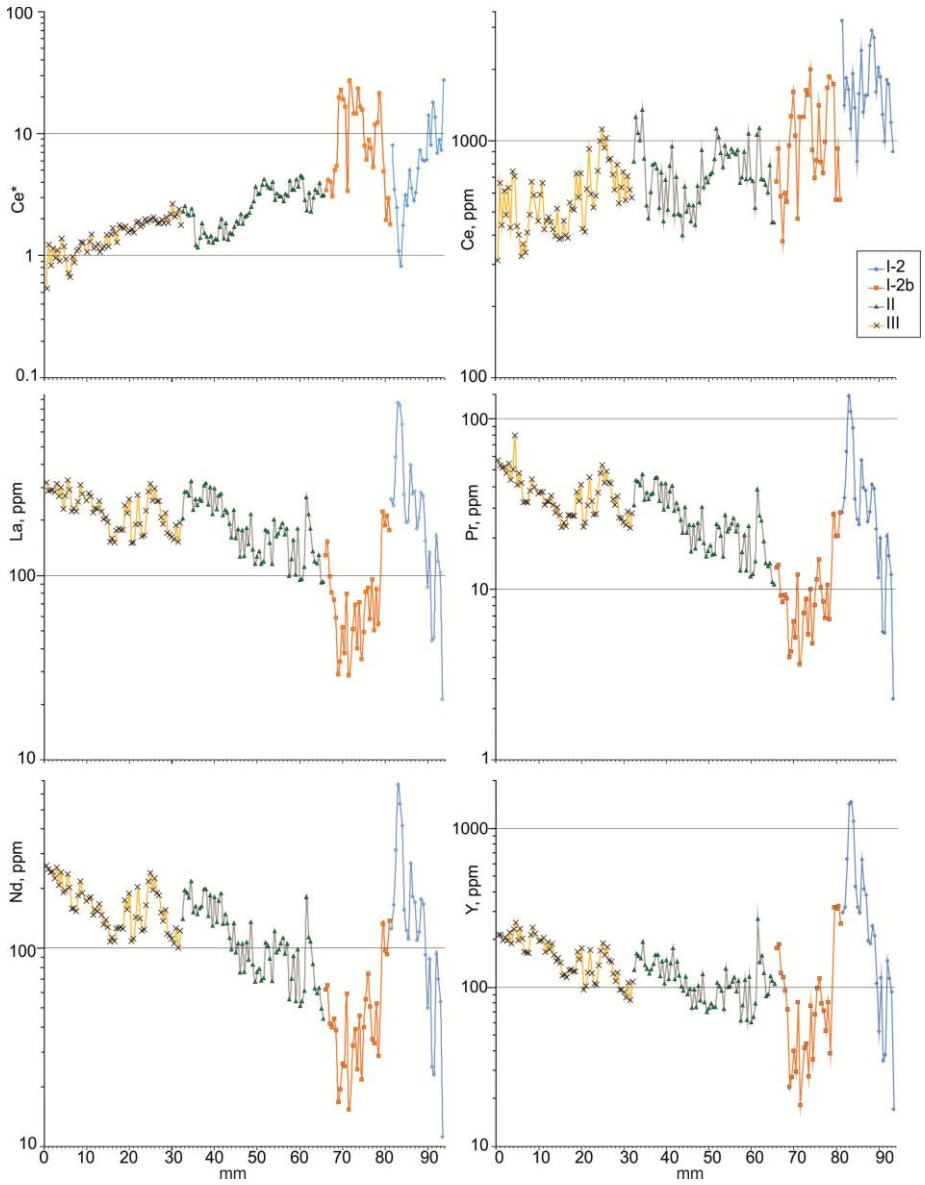

Figure 16. Variations of Ce, La, Pr, Nd, Y and Ce* in the layers (mm) of the crust from Pallada Guyot, after [55].

Experiments show that hydrogenetic Fe-Mn crusts from different oceanic regions, among which the Central Pacific, can sorb REEs from seawater into both iron and manganese components [65]. Cerium becomes oxidized and sorbed preferably on suspended matter (where it produces a positive

 doi:10.20944/preprints202510.1578.v1

anomaly) leaving the seawater depleted (negative Ce anomaly), and is thus inherited by hydrogenetic Fe-Mn crusts. In the global oceanic water depth profiles of REEs, Ce decreases gradually down from the maximum at 100–250 m below the sealevel while the concentrations of other REEs increase [57]. In this respect, the consistent variations of REE and Y (Figure 16) in the successively deposited Layers I-2b, II and III of the Pallada crust can be expected to correlate with seawater depth given that the guyot has been submerging ever deeper since the Late Oligocene.

The compositions of layers display strong correlations among Ce, La, LREE, Bi, and Ba (Figure 14) as a result of phosphatization in the CFA-enriched older layers. The apatite structure can incorporate multiple impurities by isomorphic substitutions of CO_3^{2-}, F- (as in CFA), SO_3^{2-}, Cl^- for PO_4^{3-} and Sc^{3+}, Y^{3+}, Bi^{3+} for Ca^{2+} [46]. According to LA-ICP-MS data, CFA veinlets with microinclusions of monazite, barite, and other phases in Fe-Mn crusts collected from Western and Central Pacific seamounts contain up to 3 wt% SO_3, 0.8 wt% REE (with dominant La), and minor contents of Y, Sr and Ba [64]. Cerium in CFA is much lower than other REEs, and its respective PAAS-normalized patterns typically have a negative Ce anomaly, as in the seawater [63].

There is no correlation among the highest concentrations of P, Ca, Ce, Bi, Ba, and Y in the most phosphatized Layer I-2 of the crust from Pallada Guyot, possibly because a mixture of CFA and mineral inclusions of monazite, cerianite, parisite, barite, and other carriers of P, REE, Ba, and Y fell into the 50 μm spot of the LA-ICP-MS analysis. Some of these phases, of <1 μm grain sizes, were identified earlier by microdiffraction XRD on the surfaces of crystalline CFA aggregates in phosphatized layers of Fe-Mn crusts [32]. Thus, high correlation between Ce, Ba and Bi at $r > 0.8$ (Figure 14b,d,f) may be due to the presence of these elements in Fe and Mn oxyhydroxides or to inclusions of REE carriers or phases of other trace elements (e.g., Bi) in CFA.

5.3. Co-Chronometry, Growth Rates, and Deposition History of Fe-Mn Crusts

The growth rates of Co-rich Fe-Mn crusts have multiple controls: gradual subsidence of seamounts during motions of oceanic plates, the productivity of surface waters, the pole-to-equator temperature gradient, as well as latitudinal and longitudinal mixing in the oceanic water column [43,45]. The growth rates of Fe-Mn crusts and nodules are estimated from isotopes of Th (up to 1 Myr) and Be (up to 10 Myr) [66,67]. Os-isotope stratigraphy is also used to determine the age of Fe–Mn crusts, taking into account hiatuses in their deposition, by comparing Os isotope data with the $^{187}Os/^{188}Os$ curve of seawater [67–69]. For the MST, $^{187}Os/^{188}Os$ isotope ratio was used to obtain a high-resolution isotopic record of a hydrogenetic Fe–Mn crust sampled on the southeastern slope of Il'ichev Guyot [70] and on Ita Mai Tai Guyot [71]. U–Pb CFA dating using LA-ICP-MS also clarifies the age and different stages of phosphatization of Fe-Mn crust layers [67,71].

Isotopic data ($^{230}Thex$ and $^{230}Thex/^{232}Th$ methods and $^{10}Be/^{9}Be$ chronology) were used to obtain an empirical relationship between the crust growth rate and Co contents as a basis for Co-chronometry: GR (mm per Myr) = 1.28/(Co − 0.24) [72]. This approach assumes that the Co flux to the Fe and Mn oxyhydroxides remains consistent over both time and space, but this assumption is only applicable to hydrogenetic crusts [73]. The influence of diagenetic processes on the growth rate of Fe-Mn nodules is included into an alternative Co-chronometer using Co, Fe, and Mn content [74]. Growth-rate calculations based on this Co-chronometer often yield unrealistic ages for Fe-Mn crusts, as in the case of the crust from Pallada Guyot [54], which exceed the 60 to 65 Ma biostratigraphic ages of the oldest relict layer R (Figures 2 and 3).

A shortcoming in the existing Co-chronometry approaches is that they neglect hiatuses between layers in Fe-Mn crusts, which were identified reliably from the biostratigraphy of calcareous nannoplankton, foraminifera, radiolarians, and macrofaunas (Figures 2 and 3). The available biostratigraphic constraints were used for chronostratigraphic correlations among several sections of Fe-Mn crusts from the near-equatorial Pacific [26–29,45], illustrated by a fragment in Figure 17 displaying main breaks in ore deposition for the guyots of Butakov, Alba, Fedorov, Gramberg, and Lomelik. The phosphatized Layer I-2b, well pronounced at the base of Layer II, formed during the

 doi:10.20944/preprints202510.1578.v1

Late Oligocene–Early Miocene time span (26.5 to 18 Ma) between the older and younger crust layers after a prolonged gap from 38 to 26.5 Ma in the Early to Middle Oligocene.

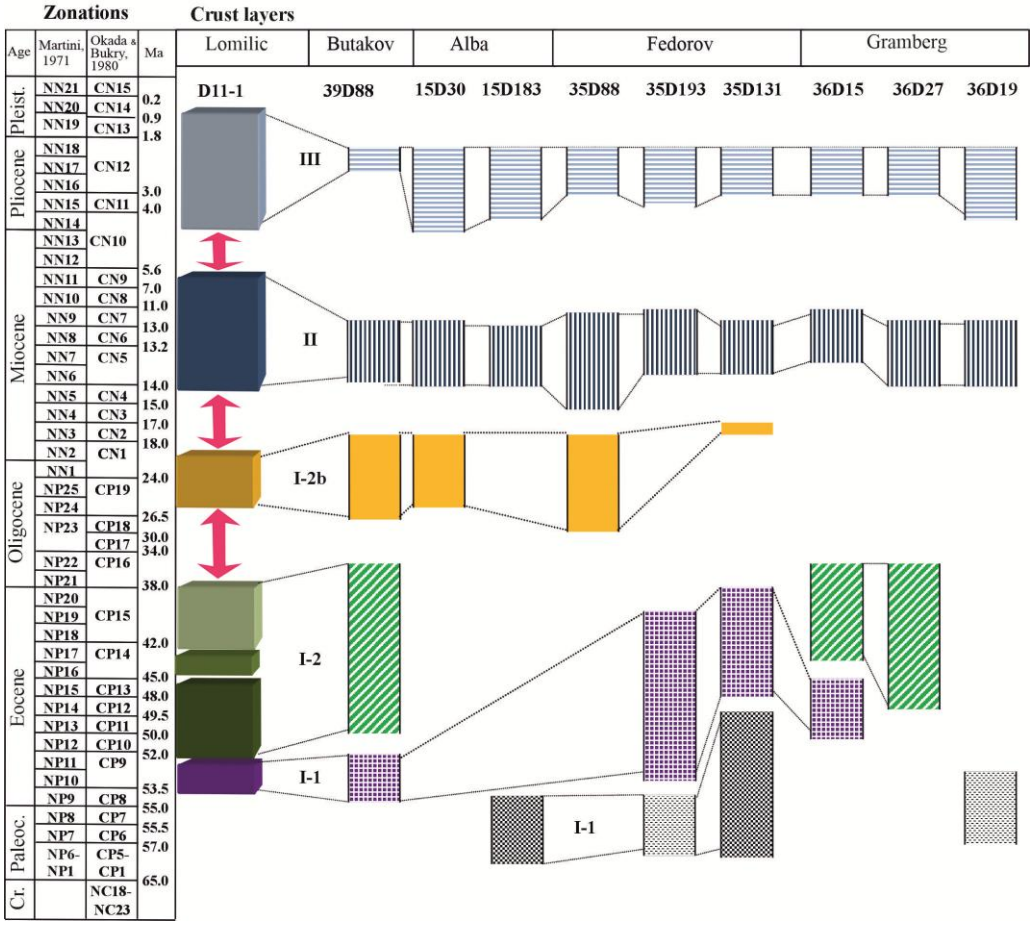

Figure 17. Chronostratigraphy of Co-rich Fe-Mn crusts from Lomilik (Marshall Islands), Butakov, Alba, Fedorov, and Gramberg guyots, modified after [29].

The principal gaps in ore deposition from the chronostratigraphic model of Figure 16 (~2 Myr in the early Pliocene between Layers II and III, ~3 Myr in the Miocene between Layers II and I-2b, and ~12 Myr in the Late Oligocene to Early Miocene between Layers I-2b and I-2) were incorporated into a new age profile for the 94 mm thick crust collected on Pallada Guyot [55]. The updated age model is presented in Figure 18a, together with growth rates from Co-chronometry [69] based on 184 EPMA analyses and the patterns of P_2O_5 and Co (Figure 18b–d). The recalculated age of the Pallada Fe-Mn crust is ~17 Myr older than that estimated by Co-chronometry (24.5 Ma, after [55] against 41.5 Ma, Figure 18a).

Layer I-2 (12 mm thick), the most phosphatized old unit in this crust, grew at about 10 mm per Myr in the Late Eocene from 41.5 to 40 Ma (Figure 18a). Its formation falls within the main Late Eocene–Early Oligocene episode of phosphogenesis in Pacific sediments, from 43 to 39 Ma [34]. The following subunit, 15 mm I-2b, formed rapidly for about 1 Myr in the Late Oligocene from 28 to 27 Ma at 10 to 70 mm per Myr, after a ~12 Myr gap. Moderate P enrichment in this layer (Figure 17c) may reflect the second phosphatization event in the Late Oligocene–Early Miocene, from 27 to 21 Ma [34]. The deposition of Layer II (32 mm) followed a ~3 Myr break and occurred in the Late Oligocene–Early Miocene, from 24 to 16 Ma, at a variable rate of 2 to 30 mm per Myr. The uppermost unit, 32 mm Layer III, was deposited after a ~2 Myr gap at a slow rate of 2 to 3 mm per Myr, from ~14 Ma to the Present and gained high Co concentrations up to 8000–10000 ppm (Figure 18d).

 doi:10.20944/preprints202510.1578.v1

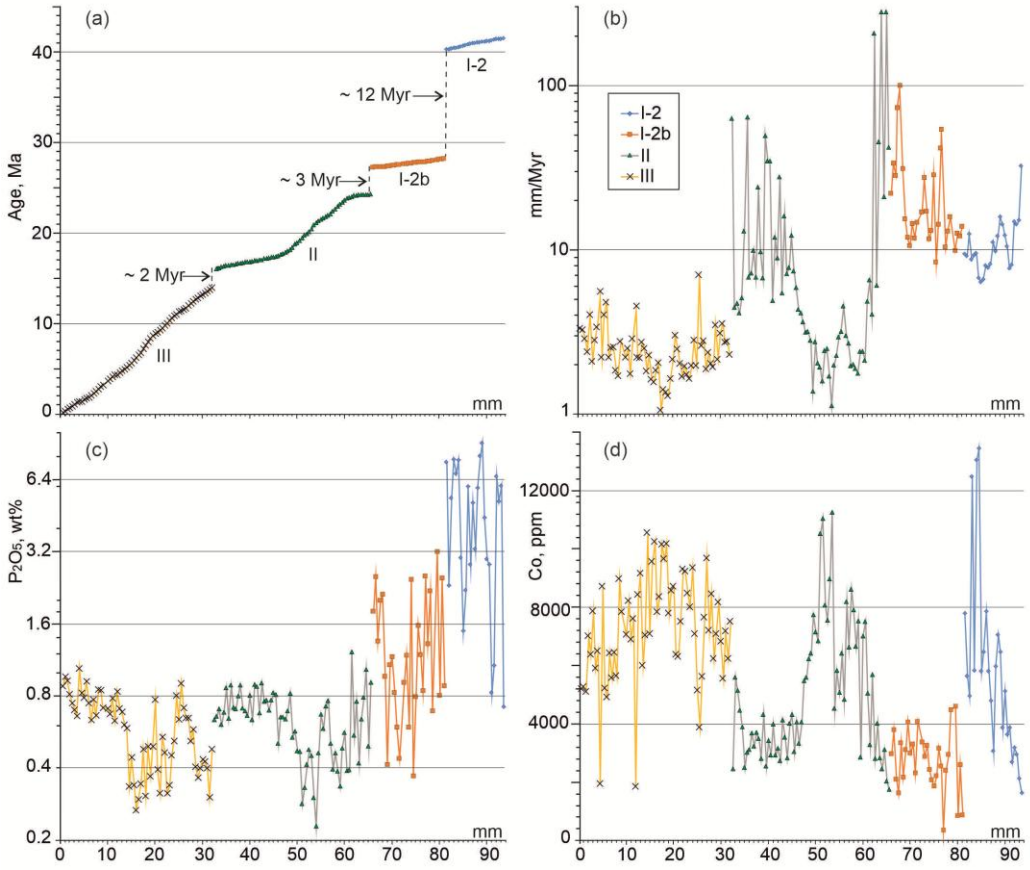

Figure 18. Age profile of the Co-rich Fe-Mn crust from Pallada Guyot (a), layer growth rates from Co-chronometry (b), and patterns of P_2O_5 (c) and Co (d).

Therefore, the Co chronometer [72] is applicable to dating layers in Co-rich Fe-Mn crusts with due regard for hiatuses revealed by chronostratigraphic correlations (Figure 17). Reliable timing on the growth history of hydrogenetic crusts requires checks against biostratigraphic data, especially identifying index species of calcareous nannoplankton. Note, however, that three to five determinations of mean Co contents for different layers of crusts from Govorov and Kocebu guyots obtained in this study (Tables A4 and A5 in Appendix A) are unsuitable for estimating the growth rates and ages of the crusts.

6. Conclusions

The precipitation history of old and young layers in Co-rich Fe-Mn crusts was inferred to correlate with global Late Cretaceous–Cenozoic climate events [6,12,26–29,43,45]. The main growth periods of Fe-Mn crusts were associated with Pacific polytaxic conditions, including warm water, increased bioproductivity, expanded OMZ, significant biogenic carbonate production, and high carbonate dissolution rates, which may have increased the Fe and Mn components in the oceanic water column. The hiatuses in the crust profiles coincide with oligotaxic ocean characterized by cool water, low bioproductivity, low planktonic calcium carbonate dissolution rates, and low Fe-Mn oxyhydroxide fluxes to the water column. In addition, regional and local factors, including geological events, hydrodynamic processes, and the morphology of guyot surfaces, created favorable conditions for accretion of Fe and Mn oxyhydroxides.

Biostratigraphic constraints place the deposition onset of Fe-Mn crusts at ~65–60 Ma. The oldest relict layer R was deposited in the Campanian–Maastrichtian and Late Paleocene near the shore, probably in the photic zone. The growth of Fe-Mn crusts continued in the Late Paleocene–Early Eocene (Layer I-1) and Middle–Late Eocene (Layer I-2) shallow-water shelf no deeper than 500–600

 doi:10.20944/preprints202510.1578.v1

m below the sealevel. The oldest unit of the crusts originated in the highly bioproductive equatorial zone. Layers II (Miocene) and III (Pliocene-Pleistocene) precipitated at larger sea depths of 1200–3000 m. The detailed stratigraphy of phosphatized sublayer I-2b, which was dated as the Late Oligocene–Early Miocene (26.5–18 Ma) and attributed to the base of Layer II, is to be further constrained. The deposition of Fe and Mn phases was interrupted several times, with the longest gap from 38 to 26.5 Ma between the old (R, I-1, and I-2) and young (I-2b, II, and III) layers of the crusts (Figures 2 and 17). The ore material of the crusts was considerably altered during the Late Eocene–Early Oligocene (43 to 39 Ma) and Late Oligocene–Early Miocene (27 to 21 Ma) global events of phosphogenesis in the Pacific sediments which left record in layers R, I-1, I-2 and sublayer I-2b, respectively. Further chronostratigrphic correlation of the Pacific Fe-Mn crusts requires support from data on index species of calcareous nannofossils at layer boundaries (Figures 3 and 17), geochemical profiles determined by localized analyses (EPMA, SEM-EDS, and LA-ICP-MS), as well as growth rates and ages of layers constrained by Co-chronometry and isotopic studies.

A major part of this study focuses on characterizing the chemistry of the Co-rich Fe-Mn crusts and their separate layers. The composition of crusts as a whole depends on the relative contributions (weight fractions) of the geochemically different constituent layers, which can be estimated using mass-balance calculations (Table 2). The amassed geochemical data for the crust layers were systematized by means of factor analysis of principal components (varimax raw) that revealed four factor groups of trace elements: (1) + (all REEs except Ce and La); (2) +(Ce, La, Ba, Mo, Sr, Pb); (3) +(Zr, Hf, Nb, Rb, As)/-Pb; (4) +(U, Th, Co, As, Sb, W)/-Y. The factor score diagrams highlight fields of elements which are especially distinctive for Layers I-1, I-2, and II+III according to factors 2 and 4 (Figure 12).

The chemistry of the Fe-Mn crusts confirms the hydrogenetic origin of Layers II and III, in which Fe and Mn oxyhydroxides precipitated directly from seawater. The older layers (R, I-1, I-2 and I-2b) most likely originated by the same mechanism but their chemistry and mineralogy were affected by later phosphatization. The contents of CFA in the phosphatized layers were estimated using the empirically found relationship between CaO and P_2O_5 (Figure 15).

The lower unit of the crusts (Layers I-1 and I-2) is enriched in Co, Y, and Ce, and its data points plot isolated fields in the Ce*–Nd and Ce*–(Y/Ho)sn diagrams (Figures 9c,d). All PAAS-normalized REE+Y patterns of hydrogenetic Fe-Mn crusts show a positive Ce anomaly and slight LREE depletion relative to HREE (Figures 9 and 10c). The consistent changes in REE and Y concentrations (decreasing Ce contents and Ce* anomaly at increasing other REEs and Y, Figure 16) toward layers I-2b → II → III in the crust from Pallada Guyot correlate with the trend of progressive ocean deepening from the Late Oligocene–Early Miocene to Present and the respective submergence of the Pacific Plate with the guyots to greater water depths. This inference has important paleogeographic implications and can be confirmed in the course of further studies on other samples of Co-rich Fe-Mn crusts.

The patterns of minor and trace elements in different layers of the crusts vary markedly between and within Govorov, Kocebu, and Pallada guyots (Figures 7, 8, 13 and 14). The heterogeneous distribution of elements in individual layers may be due to hydrodynamics of submarine currents controlled by the surface topography of guyots and the position of the Magellan Seamounts relative to the global paleoclimatic zones in the Pacific Ocean. On the other hand, the geochemistry of the Fe-Mn crusts was strongly affected by repeated episodes of Cenozoic volcanic activity in the MST area of the Pacific Plate. Specifically, voluminous eruptions of Miocene petit-spot volcanoes on the guyots [20,21], may be responsible for elevated concentrations of Nb, Zr, As, Sb and W in Layers II and III (Figures 13 and 14).

Author Contributions: Conceptualization, investigation and field sampling, I.S.P.; writing, review, and editing, all authors; Visualization, E.A.S and I.A.P. All authors have read and agreed to the published version of the manuscript.

Funding: The study was funded by grant 25–17–00128 from the Russian Science Foundation (RSF).

 doi:10.20944/preprints202510.1578.v1

Data Availability Statement: All data of this study are presented in the text, Appendix A and Supplementary Tables.

Acknowledgments: We would like to thank crew members of R/V *Gelendzhik* (JSC *Yuzhmorgeologiya*) for sampling work and support during the cruises of 2016–2017. We are grateful to our colleagues: Chubarov V.M., Zarubina O.V., and Tauson L.S. (Vinogradov Institute of Geochemistry, Irkutsk) for XRF and ICP-MS measurements.

Conflicts of Interest: The authors declare no conflict of interest.

Appendix A

Table A1. XRF analyses (wt% concentrations) of Co-rich Fe-Mn crust layers from Govorov Guyot.

	08D106					08D108			08D114			08D115			08D118		
	III	II-2	II-1	I-2	I-1	III	II-2	II-1	III	II	I-1	III	II	I-1	III	II	I-1
SiO_2	18.67	9.88	7.84	5.14	1.87	18.81	14.05	7.39	10.33	9.35	2.78	14.03	10.88	2.94	9.19	7.57	5.55
TiO_2	1.69	2.18	2.22	1.72	1.26	1.49	1.80	2.19	2.10	2.29	1.77	2.07	2.25	1.54	2.39	2.33	1.80
Al_2O_3	4.39	2.31	2.19	1.86	0.81	4.55	3.42	2.01	1.88	2.69	0.83	3.24	3.02	0.94	2.37	2.11	1.56
Fe_2O_3	28.51	25.95	22.49	15.34	13.22	27.97	27.24	23.40	29.33	21.37	18.68	27.25	24.10	15.36	23.95	22.58	19.97
MgO	1.76	1.84	2.08	2.10	1.65	1.71	1.77	1.98	1.72	2.22	1.40	1.79	1.93	1.55	1.90	2.02	1.23
MnO	22.34	30.50	33.32	35.01	31.42	22.25	26.57	33.44	29.40	35.47	31.07	25.98	30.54	30.86	32.36	34.20	24.19
CaO	3.49	3.94	4.70	10.01	18.78	3.79	3.53	4.34	3.80	4.68	14.42	3.87	3.98	16.24	3.98	4.12	16.96
Na_2O	2.55	2.14	1.87	2.11	1.73	2.18	1.73	2.12	2.01	1.96	1.47	1.83	1.88	1.56	2.17	1.76	1.36
K_2O	1.23	0.69	0.45	0.67	0.27	1.01	0.99	0.56	0.54	0.58	0.32	1.04	0.75	0.31	0.61	0.48	0.37
P_2O_5	1.06	0.96	1.22	4.23	9.42	1.05	0.98	1.03	1.03	1.07	6.70	0.97	0.98	7.92	0.82	0.79	8.70
LOI	12.38	14.77	15.30	14.51	14.62	11.70	13.67	15.02	13.81	15.18	14.15	13.73	13.85	15.12	14.95	15.57	13.59
H_2O^-	9.70	11.26	10.70	9.70	7.76	9.50	9.84	10.86	11.89	11.33	10.01	10.18	11.65	8.08	11.54	11.66	8.08
Ba	0.130	0.150	0.170	0.220	0.240	0.110	0.130	0.170	0.150	0.190	0.260	0.130	0.160	0.230	0.170	0.210	0.280
Sr	0.120	0.150	0.150	0.140	0.180	0.130	0.130	0.150	0.160	0.150	0.190	0.130	0.140	0.170	0.140	0.140	0.180
Zr	0.064	0.065	0.067	0.051	0.036	0.054	0.064	0.066	0.063	0.074	0.048	0.065	0.066	0.056	0.053	0.066	0.063
V	0.056	0.058	0.056	0.046	0.060	0.052	0.060	0.059	0.065	0.058	0.071	0.048	0.057	0.056	0.062	0.064	0.059
Co	0.400	0.590	0.670	0.590	0.440	0.350	0.490	0.590	0.580	0.690	0.350	0.610	0.660	0.500	0.840	0.650	0.240
Ni	0.300	0.470	0.600	0.840	0.600	0.280	0.390	0.590	0.380	0.710	0.380	0.360	0.540	0.570	0.530	0.640	0.290
Cu	0.085	0.119	0.156	0.188	0.106	0.059	0.107	0.178	0.066	0.236	0.123	0.088	0.159	0.162	0.205	0.208	0.133
Zn	0.047	0.055	0.068	0.088	0.086	0.048	0.055	0.067	0.060	0.079	0.068	0.050	0.064	0.077	0.071	0.085	0.075
Total	99.27	96.82	95.62	94.86	96.80	97.59	97.18	95.35	97.47	99.05	95.08	97.28	96.01	96.16	96.76	95.59	96.60
Fe	20	18	16	11	9	20	19	16	21	15	13	19	17	11	17	16	14
Mn	17	24	26	27	24	17	21	26	23	27	24	20	24	24	25	26	19
Mn/Fe	0.87	1.30	1.64	2.53	2.63	0.88	1.08	1.58	1.11	1.84	1.84	1.06	1.40	2.22	1.50	1.68	1.34

Table A2. XRF analyses (wt% concentrations) of Co-rich Fe-Mn crust layers from Kocebu Guyot.

	14D77-2					14D53			14MTP02			14MTP01
	III	II-2	II-1	I-2	I-1	III	II	I-2	III	II	I-1	I-1
SiO_2	17.67	7.70	10.44	2.14	1.82	20.49	11.36	4.75	14.96	11.26	4.89	2.76
TiO_2	1.36	1.86	2.06	1.28	1.02	1.56	2.05	1.72	1.94	2.19	1.75	1.49
Al_2O_3	3.93	1.70	2.97	0.91	0.90	5.15	3.39	1.75	2.96	3.44	1.65	1.12

 doi:10.20944/preprints202510.1578.v1

Fe_2O_3	27.36	25.36	24.64	11.71	11.86	27.94	24.31	16.92	29.53	22.10	20.60	17.77
MgO	1.74	1.91	2.05	1.68	1.76	1.78	1.98	1.82	1.62	1.97	1.37	1.28
MnO	23.53	33.75	30.51	29.32	32.72	21.29	27.87	29.54	25.23	30.71	25.79	28.58
CaO	3.42	4.12	4.24	20.26	17.90	3.73	5.43	14.20	3.51	4.14	14.04	17.70
Na_2O	2.33	1.70	1.88	2.02	1.68	1.97	1.82	1.72	1.87	1.82	1.49	1.61
K_2O	0.89	0.48	0.79	0.39	0.40	1.12	0.93	0.46	0.90	0.88	0.42	0.28
P_2O_5	1.07	1.02	1.20	10.02	8.84	1.04	1.94	6.86	0.98	0.97	6.86	8.81
LOI	13.15	15.31	14.18	14.21	14.09	11.81	14.46	14.33	13.02	15.10	16.89	13.81
H_2O^-	9.95	12.32	11.62	8.15	8.58	10.23	9.83	8.39	9.68	9.42	7.37	9.69
Ba	0.110	0.150	0.170	0.190	0.260	0.110	0.150	0.170	0.140	0.210	0.310	0.300
Sr	0.130	0.160	0.150	0.170	0.170	0.120	0.140	0.150	0.140	0.140	0.170	0.200
Zr	0.054	0.056	0.062	0.043	0.037	0.061	0.063	0.062	0.063	0.075	0.069	0.037
V	0.058	0.071	0.058	0.046	0.064	0.052	0.052	0.050	0.060	0.053	0.058	0.071
Co	0.420	0.670	0.570	0.430	0.460	0.380	0.530	0.450	0.420	0.520	0.260	0.290
Ni	0.350	0.570	0.530	0.690	0.700	0.310	0.480	0.650	0.290	0.570	0.390	0.320
Cu	0.064	0.089	0.121	0.161	0.101	0.073	0.114	0.165	0.100	0.246	0.199	0.068
Zn	0.047	0.062	0.060	0.094	0.121	0.048	0.059	0.075	0.063	0.075	0.077	0.077
Total	97.68	96.74	96.68	95.76	94.90	99.03	97.13	95.84	97.80	96.47	97.28	96.57
Fe	19	18	17	8	8	20	17	12	21	15	14	12
Mn	18	26	24	23	25	17	22	23	20	24	20	22
Mn/Fe	0.95	1.47	1.37	2.77	3.05	0.84	1.27	1.93	0.95	1.54	1.39	1.78

Table A3. ICP-MS analyses (ppm concentrations) of Co-rich Fe-Mn crust layers from Govorov Guyot.

	08D106					08D108			08D114			08D115			08D118		
	III	II-2	II-1	I-2	I-1	III	II-2	II-1	III	II	1-1	III	II	1-1	III	II	I-1
Co	4400	6506	7100	5994	4779	3988	5683	6514	6270	7014	4041	6359	7176	5337	8694	6765	2568
Ni	2962	4739	6010	7932	5586	2746	3813	5828	3563	6607	3864	3621	5332	5658	5400	6049	2908
Cr	43	14	4.3	12	35	27	22	13	12	13	32	5.8	32	22	1.9	30	25
V	555	636	634	481	658	597	606	626	661	613	799	558	599	626	681	643	688
Cu	873	1315	1777	1935	1110	743	2089	1993	766	2466	2533	960	1800	1690	2357	3275	1517
Sb	48	52	55	49	34	39	49	52	48	52	47	70	58	46	46	49	53
W	72	90	95	96	65	61	89	103	83	89	50	71	95	85	80	90	71
Mo	352	539	590	564	767	385	443	598	505	588	770	393	516	690	507	549	520
Zn	691	629	757	928	756	516	653	706	590	943	629	554	759	762	745	817	621
Be	6.0	4.3	6.2	4.7	5.5	3.6	22	6.8	5.6	6.5	27	3.1	6.6	4.8	4.6	23	15
Rb	18	14	9.4	26	1.3	16	31	31	8.9	33	1.8	12	33	12	6.7	8.9	12
Ba	1451	1797	2159	3119	3039	1400	2044	2186	1763	3126	3529	1580	2827	3097	1988	2619	3934
Th	14	14	14	6.8	8.6	17	10	16	17	9.0	9.6	15	17	10	20	14	9.6
U	11	14	13	9.1	11	11	13	15	14	11	14	12	13	11	13	11	11
Nb	64	75	79	62	42	46	69	74	59	75	45	84	79	54	67	78	52
Ta	0.33	0.31	0.44	–	–	0.05	0.33	0.47	0.49	0.83	–	0.66	0.05	–	0.75	0.75	–
Pb	146	367	1180	1483	1702	99	158	763	507	281	1343	327	547	1350	555	1440	1587
Sr	1309	1572	1649	1483	1818	1325	1310	1689	1558	1529	1996	1344	1520	1787	1519	1504	1810
Zr	627	752	728	544	391	570	664	858	588	794	494	609	738	601	529	675	637

 doi:10.20944/preprints202510.1578.v1

Hf	9.7	13	12	9.2	3.8	7.3	11	15	8.5	15	6.3	11	13	8.2	8.3	12	9.1
Ga	88	39	17	1.0	0.03	10	21	5.6	11	14	1.3	43	0.03	8.3	29	37	8.0
As	258	259	246	165	161	263	282	241	268	228	202	309	257	195	203	186	180
La	233	267	263	289	336	226	209	278	311	254	399	245	277	413	265	265	481
Ce	612	967	1205	1676	1726	568	622	1194	924	1297	1997	866	1130	1729	1153	1613	1771
Pr	50	61	61	59	55	52	46	66	74	61	72	52	58	73	67	65	84
Nd	221	259	252	255	230	225	197	274	309	262	297	219	249	320	278	272	351
Sm	46	53	54	52	43	48	41	57	63	53	52	47	50	56	56	57	61
Eu	11	13	13	12	10	12	9.8	13	17	13	12	11	12	14	15	13	15
Gd	48	56	54	59	57	49	42	57	66	59	60	50	53	71	59	57	72
Tb	6.8	7.9	7.2	7.5	7.0	7.3	6.3	7.9	9.8	7.5	7.8	6.9	7.2	9.2	8.2	7.7	9.1
Dy	41	45	43	47	44	44	38	44	55	43	46	41	44	59	46	43	59
Ho	8.8	9.3	9.2	10	10	8.7	8.0	9.2	11	9.0	10	8.8	9.1	14	9.2	8.7	13
Er	25	27	26	31	31	24	22	27	31	26	30	25	27	42	25	25	38
Tm	3.7	4.0	3.6	4.4	4.5	3.6	3.4	3.8	4.5	3.8	4.3	3.7	4.0	5.7	3.9	3.5	5.5
Yb	25	25	24	29	29	23	22	25	28	24	29	23	27	37	25	23	37
Lu	4.0	3.8	3.7	4.5	4.6	3.7	3.3	3.9	4.2	3.8	4.2	3.8	4.2	6.0	3.5	3.5	5.8
Y	204	189	199	393	458	201	173	215	224	244	278	197	230	560	174	190	523
LREE	1174	1620	1848	2343	2400	1131	1124	1882	1698	1940	2829	1439	1776	2605	1834	2285	2763
HREE	366	367	371	585	646	364	318	392	433	421	469	360	406	803	354	361	763
Ce*	1.3	1.8	2.2	3.0	2.9	1.2	1.5	2.0	1.4	2.4	2.7	1.8	2.1	2.3	2.0	2.8	2.0
L/HREE	3.2	4.4	5.0	4.0	3.7	3.1	3.5	4.8	3.9	4.6	6.0	4.0	4.4	3.2	5.2	6.3	3.6
REY	1540	1987	2218	2928	3045	1496	1442	2274	2131	2361	3298	1799	2181	3408	2189	2646	3526

Table A4. ICP-MS analyses (ppm concentrations) of Co-rich Fe-Mn crust layers from Kocebu Guyot.

	14D77-2					14D53			14MTP02			14MTP01
	III	II-2	II-1	I-2	I-1	III	II	I-2	III	II	I-1	I-1
Co	4608	6910	6419	4512	4889	4127	6085	5086	5062	5266	3102	3203
Ni	3258	5413	5200	6599	6999	3072	4903	6746	3036	5234	4034	3222
Cr	17	4.5	33	13	52	38	46	27	60	15	23	39
V	605	703	664	512	740	528	607	544	667	537	691	745
Cu	674	1003	1372	1826	1110	755	1316	1788	1171	2479	2120	760
Sb	42	49	54	34	31	46	56	49	46	48	53	47
W	68	107	86	66	40	60	83	108	65	78	93	42
Mo	431	671	563	556	804	326	477	519	399	479	563	707
Zn	498	749	784	805	1005	488	773	826	657	851	701	623
Be	5.4	3.4	5.6	8.3	1.9	4.5	6.0	5.3	6.2	7.1	8.8	5.1
Rb	16	24	44	3.7	8.9	21	46	21	11	40	7.8	1.9
Ba	1356	2285	2867	2159	3240	1340	2665	2818	1823	3071	4396	3963
Th	13	13	15	3.3	8.0	13	14	5.4	16	9.9	9.2	7.0
U	11	15	14	10	12	10	13	13	13	10	10	13
Nb	55	65	79	37	35	68	83	64	59	71	52	39
Ta	0.14	0.05	0.42	–	–	1.1	0.52	–	0.45	0.89	–	–
Pb	72	848	149	1172	1900	120	130	765	428	228	1098	2029

 doi:10.20944/preprints202510.1578.v1

Sr	1346	1720	1660	1603	1726	1202	1578	1595	1497	1346	1838	2071
Zr	537	643	758	437	388	561	749	674	630	834	691	391
Hf	8.0	9.6	13	5.9	4.1	9.5	13	12	9.6	16	9.3	4.4
Ga	11	17	5.4	0.03	2.4	56	17	2.6	11	11	15	5.7
As	271	305	297	136	160	257	271	207	292	222	191	209
La	213	276	283	338	252	187	239	254	310	228	421	418
Ce	535	842	978	1258	1355	583	981	1333	969	1212	1625	2177
Pr	43	61	62	58	43	37	50	53	73	55	75	56
Nd	195	259	263	263	185	160	215	227	311	230	314	229
Sm	37	53	56	49	33	33	42	44	64	48	59	38
Eu	9.8	13	13	12	8.1	8.3	11	11	16	11	14	9.1
Gd	41	52	57	59	43	36	49	52	66	48	66	53
Tb	6.0	7.7	7.8	7.7	5.6	5.3	6.4	6.6	9.4	6.5	8.0	6.5
Dy	37	47	46	49	35	32	37	39	55	38	51	42
Ho	7.7	9.4	9.6	12	8.6	7.1	8.5	8.8	11	7.7	11	9.9
Er	23	27	28	34	26	21	24	25	30	22	34	31
Tm	3.4	3.9	4.1	5.0	3.9	3.1	3.7	3.7	4.5	3.2	4.8	4.3
Yb	22	26	26	32	25	20	24	23	28	20	31	28
Lu	3.4	4.0	4.0	5.0	4.3	3.4	3.9	3.9	4.4	3.3	4.7	4.5
Y	189	186	235	536	333	176	247	321	230	195	434	439
LREE	1032	1504	1654	1977	1876	1008	1537	1922	1742	1783	2507	2927
HREE	332	362	417	740	485	304	403	483	439	344	644	619
Ce*	1.3	1.5	1.7	2.1	3.0	1.6	2.1	2.7	1.5	2.5	2.1	3.2
L/HREE	3.1	4.1	4.0	2.7	3.9	3.3	3.8	4.0	4.0	5.2	3.9	4.7
REY	1364	1866	2072	2717	2361	1312	1941	2405	2181	2127	3151	3546

Table A5. Bulk chemistry of MST Co-rich Fe-Mn crusts.

	Mean	Var,%	n	Mean	Mediana	Min	Max	Var,%	n
Mn	*21.13*	*13*	*803*						
Fe	*16.28*	*13*	*794*						
P_2O_5	*2.75*	*71*	*631*						
Mn/Fe	*1.31*	*17*	*793*						
Co	*5800*	*23*	*803*	5498	5400	2700	9000	19	276
Ni	*4400*	*18*	*803*	4307	4300	1200	6700	19	276
Cr	*17*	*107*	*309*	17	11	2.4	720	277	248
V	*529*	*13*	*247*	500	500	260	625	9.4	146
Cu	*1200*	*26*	*803*	1220	1200	520	2113	21	276
Sc	*10.4*	*37*	*309*	10	10	1.0	25	31	270
Sn	*8.5*	*38*	*309*	8.3	8.3	2.9	15	22	274
Sb	*39*	*23*	*309*	36	36	9.2	60	21	276
W	*62*	*29*	*309*	71	71	14	120	24	276
Mo	*383*	*20*	*309*	378	370	140	600	19	276
Tl	*124*	*25*	*309*	122	122	44	190	22	274

 doi:10.20944/preprints202510.1578.v1

Zn	*555*	*16*	*309*	550	560	320	801	19	276
Li	*4.7*	*56*	*305*	5.2	4.5	1.5	16.7	48	274
Be	*5.8*	*38*	*309*	5.4	4.9	2.2	15	42	276
Cs	*0.50*	*48*	*309*	0.54	0.50	0.09	1.5	46	274
Rb	*9.2*	*44*	*309*	8.9	8.4	3	34	38	276
Ba	*1528*	*21*	*309*	1377	1400	740	4700	27	276
Th	*13*	*29*	*309*	14	13	4.9	27	33	276
U	*11*	*23*	*309*	12	12	5.9	21	19	276
Nb	*40*	*53*	*309*	41	42	7.3	94	37	276
Ta	*0.60*	*69*	*309*	0.47	0.38	0.09	1.9	61	275
Pb	*1166*	*20*	*309*	1121	1100	352	1700	21	276
Sr	*1278*	*14*	*309*	1252	1300	686	1714	13	276
Zr	*321*	*93*	*309*	231	120	14	1200	106	276
Hf	*4.2*	*96*	*309*	3.0	1.8	0.40	17	94	276
Bi	*35*	*30*	*309*	41	40	16	82	26	274
Ga	*14*	*66*	*309*	13	13	0.03	25	30	276
As	*193*	*59*	*309*	162	160	92	260	17	276
Cd	*3.9*	*47*	*309*	4.1	4.1	1.6	6.3	17	274
Te	*57*	*35*	*309*	51	49	14	98	26	274
La	*272*	*19*	*309*	242	240	124	410	22	276
Ce	*972*	*25*	*309*	849	820	390	1700	26	276
Pr	*52*	*20*	*309*	46	45	27	75	21	276
Nd	*212*	*21*	*309*	203	200	130	280	16	276
Sm	*43*	*21*	*309*	43	42	28	64	17	276
Eu	*11*	*19*	*309*	11	11	6.9	16	16	276
Gd	*55*	*21*	*309*	54	54	28	78	16	276
Tb	*7.7*	*18*	*309*	7.8	7.7	4.3	11	15	276
Dy	*46*	*21*	*309*	46	46	21	65	14	276
Ho	*9.6*	*19*	*309*	9.5	9.4	4.3	13	14	276
Er	*28*	*20*	*309*	27	27	12	40	14	276
Tm	*4.0*	*18*	*309*	4.0	3.9	1.8	5.6	14	276
Yb	*26*	*20*	*309*	25	25	12	36	14	276
Lu	*4.1*	*20*	*309*	4.1	4.0	1.8	6.2	14	276
Y	*230*	*32*	*309*	216	200	86	450	32	276
LREE	*1562*		*309*	1394	1365	743	2525	22	276
HREE	*180*		*309*	178	176	85	254	14	276
Ce*	*1.9*		*309*	1.8	1.8	1.0	2.7	15	276
L/HREE	*8.7*		*309*	7.8	7.7	5.1	12	18	276
REY	*1972*		*309*	1788	1760	1007	3229	21	276

Notes. Mn, Fe, and P_2O_5 are in wt%, trace elements are in ppm. Italicized colored values refer to statistical parameters for bulk crusts chemistry from Govorov, Kocebu, Il'ichev, Pegas, Alba, Pallada, Fedorov, Gramberg, Ita Mai Tai, Gelendzhik, and Butakova guyots, after [47]; other data are explained in text, statistical parameters for bulk crusts chemistry from Govorov, Kocebu, Vulkanolog, Skornyakova, Pegas, Il'ichev, Pallada,

 doi:10.20944/preprints202510.1578.v1

Gelendzhik, Butakov, and several guyots east of MST (Zatonsky, Nazimov, Zubov, Marova, and Rykachev), see guyots sites on https://www.ngdc.noaa.gov/gazetteer/. Var,% = variance; Min and Max = minimum and maximum element concentrations; n = number of analyses in the dataset.

Table A6. Minor and trace element chemistry of MST Co-rich Fe-Mn crust layers III and II.

	III						II					
	Mean	Mediana	Min	Max	Var,%	n	Mean	Mediana	Min	Max	Var,%	n
Fe	*17.69*				*10*	*139*	*17.10*				*14*	*131*
Mn	*23.67*				*13*	*140*	*22.35*				*13*	*140*
P_2O_5	*1.21*				*65*	*128*	*1.60*				*74*	*123*
TiO_2	*1.77*				*18*	*64*	*1.82*				*17*	*60*
Mn/Fe	*1.34*				*19*	*139*	*1.35*				*25*	*130*
Co	5654	5600	3200	9200	28	31	5535	5683	3200	7176	22	33
	6500				*24*	*140*	*5200*				*24*	*131*
Ni	4023	4000	2559	5800	25	31	4838	4900	3270	6607	19	33
	4700				*22*	*140*	*5000*				*22*	*131*
Cr	20	20	1.9	60	78	18	21	22	4.2	46	59	20
V	602	597	510	690	11	17	607	607	508	703	8	20
Cu	869	810	340	2357	46	31	1547	1500	700	3275	34	33
	1030				*45*	*140*	*1680*				*27*	*131*
Sc	8.0	7.3	4.3	13	35	20	8.4	7.8	4.3	13	25	22
Sn	7.8	7.9	5.5	10	18	23	11	12	6.8	15	18	22
Sb	41	39	31	70	19	31	44	44	26	61	19	33
W	90	90	53	124	21	31	91	91	57	142	20	33
Mo	459	440	320	640	20	31	484	479	270	671	20	33
	500				*20*	*59*	*460*				*21*	*43*
Tl	136	127	80	230	31	23	152	146	65	230	29	22
Zn	566	580	370	745	15	31	701	730	460	943	16	33
	630				*25*	*38*	*710*				*13*	*37*
Li	2.9	2.0	0.97	8.8	69	23	5.1	4.7	1.6	10	53	22
Be	4.8	4.3	3.1	8.2	29	31	6.8	6.0	3.4	23	63	33
Cs	0.38	0.27	0.07	1.2	84	23	0.59	0.65	0.11	1.5	63	22
Rb	8.5	7.4	3.1	21	58	31	15	10	3.2	46	83	33
Ba	1351	1300	863	1988	20	31	1843	1797	994	3126	33	33
Th	14	14	6.6	22	32	31	10	10	2.6	17	45	33
U	13	14	10	19	14	31	12	13	9.4	16	14	33
Nb	55	53	32	88	26	31	59	61	17	91	31	33
Ta	0.50	0.41	0.05	1.2	62	31	0.49	0.40	0.05	1.7	70	33
Pb	1051	1127	72	1682	49	31	887	966	130	1530	44	33
	1500				*16*	*38*	*1220*				*16*	*37*
Sr	1419	1458	1100	1731	12	31	1463	1500	1000	1769	12	33
Zr	329	230	45	877	78	31	430	380	35	1100	83	33
Hf	5.0	2.9	0.7	11	74	31	6.9	5.3	0.77	17	82	33
Bi	32	31	20	54	28	23	36	37	20	69	33	22

 doi:10.20944/preprints202510.1578.v1

Ga	16	11	5.4	88	107	31	13	11	0.03	39	61	33
As	232	230	130	343	24	31	207	212	72	305	26	33
Cd	4.0	4.1	2.9	5.1	16	23	4.0	4.0	2.7	5.4	19	22
Te	43	43	26	68	26	23	55	53	30	95	26	22
La	231	226	146	320	20	31	221	220	130	300	23	33
	290				*17*	*22*	*257*				*17*	*24*
Ce	696	690	400	1153	27	31	860	770	420	1613	33	33
	881				*29*	*22*	*903*				*22*	*24*
Pr	50	50	34	74	22	31	49	50	29	66	22	33
	60				*22*	*22*	*50*				*16*	*24*
Nd	218	219	148	311	20	31	212	215	120	274	21	33
	237				*21*	*22*	*202*				*16*	*24*
Sm	45	46	30	64	21	31	44	46	24	57	23	33
	52				*23*	*22*	*43*				*16*	*24*
Eu	12	11	7.0	17	21	31	11	11	6.4	15	20	33
	12				*22*	*22*	*10*				*14*	*24*
Gd	56	54	35	80	20	31	51	51	31	79	19	33
	65				*21*	*22*	*57*				*16*	*24*
Tb	8.0	7.7	5.3	12	20	31	7.2	7.3	4.6	10	19	33
	9.0				*21*	*22*	*8.0*				*17*	*24*
Dy	48	46	32	67	18	31	42	43	27	59	17	33
	55				*25*	*22*	*46*				*20*	*24*
Ho	9.6	9.2	6.7	14	16	31	8.5	8.6	5.6	11	15	33
	12				*29*	*22*	*10*				*23*	*24*
Er	28	27	19	40	16	31	25	25	16	33	15	33
	33				*31*	*22*	*30*				*24*	*24*
Tm	4.1	3.9	2.9	5.9	15	31	3.5	3.6	2.4	4.5	15	33
	5.0				*29*	*22*	*4.0*				*23*	*24*
Yb	26	26	20	36	13	31	23	24	16	28	14	33
	32				*39*	*22*	*29*				*26*	*24*
Lu	4.1	4.1	3.1	5.6	13	31	3.6	3.7	2.6	4.4	13	33
	5.0				*40*	*22*	*5.0*				*27*	*24*
Y	167	170	94	230	18	31	167	170	92	247	26	33
	189				*20*	*22*	*231*	–	–	–	*35*	*24*
LREE	1252	1174	808	1834	22	31	1396	1297	743	2285	27	33
	1532					*22*	*1465*					*24*
HREE	183	177	123	257	17	31	164	167	105	229	16	33
	216					*22*	*189*					*24*
Ce*	1.5	1.4	1.1	2.0	19	31	1.9	1.8	1.4	2.8	21	33
	1.5					*22*	*1.8*					*24*
L/HREE	6.9	6.9	4.8	10	20	31	8.5	7.7	6.2	13	23	33
	7.1					*22*	*7.8*					*24*
REY	1602	1506	1111	2189	19	31	1727	1593	958	2646	24	33
	1937					*22*	*1775*					*24*

 doi:10.20944/preprints202510.1578.v1

Notes. Mn, Fe, TiO_2, and P_2O_5 are in wt%, trace elements are in ppm. Italicized colored values refer to statistical parameters of chemistry for crust layers III and II from Govorov, Kocebu, Il'ichev, Pegas, Alba, Pallada, Fedorov, Gramberg, Ita Mai Tai, Gelendzhik, and Butakov guyots, after [47]; other data are explained in text, statistical parameters for chemistry for crust layers III and II from Govorov, Kocebu, Vulkanolog, Gelendzhik, and Butakov guyots. Var,% = variance; Min and Max = minimum and maximum element concentrations; n = number of analyses in the dataset.

Table A7. Minor and trace element chemistry of MST Co-rich Fe-Mn crust layers I-2 and I-1.

	I-2						I-1					
	Mean	Mediana	Min	Max	Var,%	n	Mean	Mediana	Min	Max	Var,%	n
Fe	*11.17*				*26*	*106*	*12.40*				*22*	*89*
Mn	*17.96*				*20*	*107*	*21.95*				*15*	*89*
P_2O_5	*9.74*				*47*	*97*	*6.93*				*38*	*84*
TiO_2	*0.72*				*56*	*51*	*0.79*				*66*	*37*
Mn/Fe	*1.68*				*25*	*106*	*1.85*				*26*	*89*
Co	3066	2949	1000	5994	41	25	3914	4000	2400	5337	21	29
	3200				*31*	*107*	*4100*				*23*	*89*
Ni	4597	4092	2300	7932	38	25	4132	3864	1800	7600	35	29
	4500				*31*	*107*	*4200*				*29*	*89*
Cr	13	13	3.0	27	63	22	18	22	1.5	52	80	26
V	445	456	293	549	19	12	673	688	440	880	15	15
Cu	1377	1300	890	2400	27	25	1106	981	400	2533	45	29
	1430				*27*	*107*	*1170*				*31*	*88*
Sc	10	10	6.4	17	28	22	7.1	5.9	3.2	23	59	22
Sn	9.3	9.5	4.1	15	31	22	7.8	8.0	3.8	13	29	22
Sb	23	18	9.7	49	55	25	30	29	13	53	39	29
W	61	58	23	108	41	25	44	41	20	93	43	29
Mo	383	384	180	642	32	25	580	580	320	840	26	29
	460				*26*	*21*	*650*				*16*	*18*
Tl	122	110	46	217	42	22	125	119	77	195	29	22
Zn	624	590	350	1034	32	25	724	701	370	1435	33	29
	640				*23*	*21*	*730*				*22*	*22*
Li	3.5	3.1	2.0	6.7	37	22	2.1	1.6	0.84	6.8	76	22
Be	4.8	4.4	2.0	8.3	30	25	6.3	5.1	1.9	27	74	29
Cs	0.39	0.41	0.10	0.84	51	22	0.16	0.14	0.06	0.47	63	22
Rb	6.9	5.4	3.2	26	76	25	4.7	4.0	1.3	12	55	29
Ba	1535	1300	950	3119	37	25	2528	2318	1266	4396	35	29
Th	5.3	3.9	2.2	24	87	25	11	11	3.1	19	34	29
U	10	10	7.4	13	14	25	12	12	8.9	17	15	29
Nb	27	20	5.3	66	68	25	29	22	9.3	54	48	29
Ta	0.50	0.44	0.13	1.2	66	22	0.49	0.42	0.10	1.1	60	22
Pb	879	810	550	1483	30	25	1596	1638	788	2300	25	29
	1050				*36*	*21*	*1840*				*22*	*22*
Sr	1525	1595	1100	1800	11	25	1764	1779	1300	2252	12	29

 doi:10.20944/preprints202510.1578.v1

Zr	275	190	55	674	75	25	250	155	10	691	85	29
Hf	4.7	3.2	0.88	12	78	25	3.5	2.5	0.44	11	83	29
Bi	45	42	25	81	34	22	77	81	45	109	21	22
Ga	8.9	9.3	0.03	16	47	25	11	12	0.03	21	45	29
As	133	130	72	207	22	25	163	161	110	225	18	29
Cd	3.3	3.2	1.4	6.3	37	22	3.4	3.3	1.9	5.2	28	22
Te	49	49	26	81	30	22	59	57	37	88	23	22
La	224	200	146	433	30	25	290	272	130	481	31	29
	294				*23*	*27*	*345*				*17*	*17*
Ce	854	758	440	1676	37	25	1455	1483	849	2177	23	29
	953				*24*	*27*	*1634*				*18*	*17*
Pr	42	41	26	63	25	25	50	45	29	84	29	29
	51				*36*	*27*	*56*				*18*	*17*
Nd	185	179	110	306	26	25	215	210	117	351	27	29
	209				*39*	*27*	*219*				*19*	*17*
Sm	35	34	21	52	25	25	39	37	22	61	27	29
	43				*44*	*27*	*42*				*20*	*17*
Eu	9.2	8.9	5.8	13	22	25	10	9.7	6.2	15	24	29
	11				*42*	*27*	*10*				*15*	*17*
Gd	49	47	35	71	21	25	55	53	29	89	25	29
	61				*37*	*27*	*63*				*14*	*17*
Tb	6.7	6.6	4.3	9.9	20	25	7.1	7.0	4.5	11	20	29
	8.0				*49*	*27*	*7.0*				*21*	*17*
Dy	42	42	28	63	20	25	44	42	28	69	21	29
	53				*53*	*27*	*49*				*25*	*17*
Ho	9.2	9.0	6.3	15	19	25	9.5	8.7	6.2	15	21	29
	12				*51*	*27*	*11*				*27*	*17*
Er	28	28	19	44	19	25	29	27	18	47	21	29
	38				*50*	*27*	*34*				*30*	*17*
Tm	3.9	3.9	2.8	6.2	18	25	4.1	3.9	2.7	6.5	20	29
	5.0				*48*	*27*	*5.0*				*26*	*17*
Yb	26	25	18	41	18	25	27	26	18	41	19	29
	36				*53*	*27*	*33*				*30*	*17*
Lu	4.2	4.1	3.0	6.7	18	25	4.3	4.2	3.0	7.0	20	29
	6.0				*51*	*27*	*5.0*				*34*	*17*
Y	306	272	170	718	38	25	272	210	130	560	49	29
	393				*32*	*27*	*308*				*31*	*17*
LREE	1350	1224	821	2343	32	25	2059	2020	1316	2927	22	29
	1561					*27*	*2306*					*17*
HREE	168	167	117	256	19	25	179	173	109	268	20	29
	219					*27*	*207*					*17*
Ce*	2.0	1.9	1.4	3.0	17	25	2.9	2.9	1.5	4.5	22	29
	1.8					*27*	*2.7*					*17*
L/HREE	7.9	7.4	5.7	12	21	25	12	12	5.6	16	20	29

 doi:10.20944/preprints202510.1578.v1

REY	*7.1*					*27*	*11*					*17*
	1825	1620	1201	3183	30	25	2510	2403	1648	3546	22	29
	2173					*27*	*2821*					*17*

Notes. Mn, Fe, TiO_2, and P_2O_5 are in wt%, trace elements are in ppm. Italicized colored values refer to statistical parameters of chemistry for crust layers I-2 and I-1 from Govorov, Kocebu, Il'ichev, Pegas, Alba, Pallada, Fedorov, Gramberg, Ita Mai Tai, Gelendzhik, and Butakov guyots, after [47]; other data are explained in text, statistical parameters for chemistry of crust layers I-2 and I-1 from Govorov, Kocebu, Vulkanolog, Gelendzhik, and Butakov guyots. Var,% = variance; Min and Max = minimum and maximum element concentrations; n = number of analyses in the dataset.

References

1. Lisitsyn, A.P. (Ed.) *Ferromanganese Crusts and Nodules on Seamounts of the Pacific;* Nedra: Moscow, Russia, 1990; 227p. (in Russian)
2. Baturin, G.N. *Oceanic Mineral Resources;* Nauka: Moscow, Russia, 1993; 303p. (in Russian)
3. Andreev, S.I. (Ed.) *Cobalt-Bearing Ferromanganese Crusts and Nodules of the Pacific Ocean;* VNIIOkeangeologiya: St-Petersburg, Russia, 1993; 190p. (In Russian)
4. Andreev, S.I. (Ed.) *Cobalt-Rich Ores of the World Ocean;* VNIIOkeangeologiya: St. Petersburg, Russia, 2002; 168p. (in Russian)
5. Hein, J.R.; Mizell, K.; Koschinsky, A.; Conrad, T.A. Deep-ocean mineral deposits as a source of critical metals for high- and green-technology applications: Comparison with land-based resources. *Ore Geol. Rev.* **2013**, *51*, 1–14. DOI:10.1016/j.oregeorev.2012.12.001
6. Halbach, P.E.; Jahn, A.; Cherkashov, G. Marine Co-Rich Ferromanganese Crust Deposits: Description and Formation, Occurrences and Distribution, Estimated World-wide Resources. In: Sharma, R., (Ed.) *Deep-Sea Mining: Resource Potential, Technical and Environmental Considerations*; Springer International Publishing: Cham, Switzerland, **2017**; 65–141. DOI:10.1007/978-3-319-52557-0_3
7. Bogdanov, Y.A.; Sorokhtin, O.G.; Zonenshain, L.P.; Kuptsov, V.M.; Lisitsyna, N.A.; Podrazhansky, A.M. *Ferromanganese Crusts and Nodules on Pacific Seamounts;* Nauka: Moscow, Russia, 1990; 229p. (In Russian)
8. Bogdanov, Yu.A.; Gurvich, E.G.; Bogdanova, O.Yu.; Dubinin, A.V.; Gorshkov, A.I.; Jansa, L.F. Ferromanganese crusts and nodules from guyots of the Northwestern Pacific. *Geochem. Int.* **1998,** *36(5*), 455–466.
9. Melnikov, M.E. *Deposits of Cobalt-Rich Manganese Crusts;* FGUGP GNTs; Yuzhmorgeologiya: Gelendzhik, Russia, 2005; 230p. (In Russian)
10. Melnikov, M.E. *Cobalt-rich ferromanganese crusts;* In World Ocean. V.III. Solid Minerals and Gas Hydrates in the Ocean; Nauchny Mir: Moscow, Russia, 2018; pp.285–322. (In Russian)
11. Volokhin, Y.G.; Melnikov, M.E.; Shkolnik, E.L.; Vasiliev, B.I.; Govorin, I.N.; Khersberg, L.B.; Zadornov, M.V.; Baturin, G.N.; Mechetin, A.V.; Chudaev, O.V.; et al. Guyots of the Western Pacific and their Mineralization; Nauka: Moscow, Russia, 1995; 368p. (In Russian)
12. Pletnev, S.P.; Melnikov, M.E.; S'edin, V.T.; Sedysheva, T.E.; Avdonin, V.V.; Anokhin, V.M.; Zakharov, Y.D.; Punina, T.A.; Smirnova, O.L. Geology of Guyots in the Magellan Seamounts (Pacific Ocean); Dalnauka: Vladivostok, Russia, 2020; 200p. (In Russian)
13. Melnikov, M.Y.; Pletnev, S.P.; Anokhin, V.M.; Sedysheva, T.E.; Ivanov, V.V. Volcanic edifice on guyots of the Magellan Seamounts (Pacific Ocean). *Russ. J. Pacific Geol*. **2016**, 10(6), 435–4452. DOI:10.1134/S1819714016060038
14. Melnikov, M.Y.; Podschuveit, V.B.; Pulyaeva, I.A.; Nevretdinov, E.B. Middle Miocene volcanic structures on the Dalmorgeologiya Guyot (Magellan Seamounts, Pacific Ocean). *Russ. J. Pacific Geol.* **2000**, 19, 38–46. (In Russian)
15. Koppers, A.A.P.; Staudigel, H.; Wijbrans, J.R.; Pringle, M.S. The Magellan seamount trail: Implications for Cretaceous hotspotvolcanism and absolute Pacific Plate motion. *Earth Planet. Sci. Lett. (EPSL).* **1998**, 163, 53–68. DOI:10.1016/S0012-821X(98)00175-7

16. Koppers, A.A.P.; Staudigel, H.; Wijbrans, J.R. Dating crystalline groundmass separates of altered Cretaceous seamount basalts by the $^{40}Ar/^{39}Ar$ incremental heating technique. *Chem. Geol.* **2000**, 166, 139–158. DOI:10.1016/S0009-2541(99)00188-6
17. Wei, H.; Zhang, G.-L.; Zhang, J.; Shi, X.-F.; Castillo, P.R.; Zhang, Y.; Zhang, W.-F.; Xu, Y.-G.; Li, H.-Y.; Zhang, H. Overlapping hotspot tracks and melts from diffuse plume materials in the upper mantle generated intraplate seamount groups in the WestPacific. *Earth Planet. Sci. Lett. (EPSL).* **2024**, 643, 118901. DOI:10.1016/j.epsl.2024.118901
18. Peretyazhko, I.S.; Savina, E.A. Chemistry and crystallization conditions of minerals in metasomatized oceanic lithosphere and basaltic rocks of Govorov Guyot, Magellan Seamounts, Pacific Ocean. *Minerals* **2022**, 12, 1305. DOI:10.3390/min12101305
19. Peretyazhko, I.S.; Savina, E.A. Cretaceous intraplate volcanism of Govorov Guyot and formation models of the Magellan seamounts, Pacific Ocean. *Intern. Geol. Rev.* **2023**, 65, 2479–2505. DOI:10.1080/00206814.2022.2145512
20. Peretyazhko, I.S.; Savina, E.A.; Pulyaeva, I.A.; Yudin, D.S. Intraplate volcanism of the Alba Guyot. Geodynamic formation models of the Magellan Seamounts in the Pacific Ocean for 100 million years. *Russ. Geol. Geophys*. **2023**, 64, 1–27. DOI:10.2113/RGG20214422
21. Peretyazhko, I.S.; Savina, E.A.; Pulyaeva, I.A. Miocene petit-spot basanitic volcanoes on Cretaceous Alba Guyot (Magellan Seamount Trail, Pacific Ocean). *Geosciences* **2024**, 14, 2522. DOI:10.3390/geosciences14100252
22. Avdonin, V.V.; Kruglyakov, V.V.; Lygina, T.I.; Melnikov, M.E.; Sergeeva, N.E. *Oceanic Ferromanganese Ores: Genetic Interpretation of Structures and Textures;* GEO: Moscow, Russia, 2014; p. 164. (in Russian)
23. Melnikov, M.E.; Pulyaeva, I.A. Ferromanganese crusts deposits of Marcus-Wake and Magellan seamount, Western Pafic: structure, composition and age. *Russ. J. Pac. Geol.*, **1995**, 11, 525.
24. Melnikov, M.E.; Pletnev, S.P. Age and formation conditions of the Co-rich manganese crust on guyots of the Magellan Seamounts. *Lithol. Miner. Resour.* **2013**, *48(1),* 1–13.
25. Pletnev, S.P.; Smirnova, O.L.; Melnikov, M.E.; Punina, T.A.; Kopaevich, L.F. New paleontological data on Govorov, Vulkanolog, and Kocebu guyots (Magellan seamounts, Pacific). *Russ. J. Pac. Geol.* **2017**; *11(2),* 148–153. DOI:10.1134/S1819714017020063
26. Pulyaeva, I.A. Stratification of ferromanganese crusts on the Magellan seamounts. *In: Proc. 30th International Geological Congress;* Beijing, China, **1996**, *13*, 111–128.
27. Pulyaeva, I.A.; Hein, J.R. Paleoceanographic conditions during the formation of Fe-Mn crusts from the Pacific Ocean: Biostratigraphic and compositional evidence. *In: Abstracts and Proceedings, 39th Underwater Mining Institute*; Gelendzhik, Russia, **2010,** 1–12. (in Russian)
28. Pulyaeva, I.A.; Hein, J.R. Chronostratigraphy of Fe-Mn crusts from the Pacific Ocean. *In: Proc. Joint International Conference on Minerals of the Ocean-5 and Deep-Sea Minerals and Mining-3;* St. Petersburg, Russia, **2010**, 38–40. (in Russian)
29. Pulyaeva, I.A.; Hein, J.R. Hydrogenetic Fe-Mn crusts from the Atlantic and Pacific oceans: Geological evolution and conditions of formation. *In: Marine Minerals: Recent Innovations in Technology; UMI:* Anaheim, CA, USA, 2011.
30. Avdonin, V.V.; Sergeeva, N.E. Formation patterns of ferromanganese crusts and nodules. *Bull. Moscow State Univ. Ser. 4: Geol*. **2003**, *5*, 31–39. (in Russian)
31. Bogdanova, O.Yu.; Novikov, G.V.; Bogdanov, Yu.A.; Gorshkov, A.I. Mineralogy and morphogenetic types of ferromanganese deposits in the World ocean. *Geol. Ore Dep*. **2008,** *50(6),* 462–469.
32. Baturin, G.N.; Dubinchuk, V.T.; Azarnova, L.A.; Mel'nikov, M.E. Minerals of rare earth elements in the phosphate fraction of ferromanganese crusts on seamounts. *Dokl. Earth Sci.* **2006**, *411 (9)*, 1362-1365. DOI:10.1134/S1028334X06090066
33. Hein; J.R., Koschinsky, A.; Bau, M.; Manheim, F.T.; Kang, J.-K.; Roberts, L., Cobalt-rich ferromanganese crusts in the Pacific. *Handbook of Marine Mineral Deposits* **2000**, *18*, pp.239–273.
34. Hein, J.R.; Yeh, H.-W.; Gunn, S.H.; Sliter, W.V.; Benninger, L.M.; Wang, C.-H. Two major Cenozoic episodes of phosphogenesis recorded in equatorial Pacific seamount deposits. *Paleoceanography* **1993**, *8*, 293–311. DOI 10.1029/93PA00320

 doi:10.20944/preprints202510.1578.v1

35. Koschinsky, A.; Stascheit, A.; Bau, M.; Halbach, P. Effects of phosphatization on the geochemical and mineralogical composition of marine ferromanganese crusts. *Geochim. Cosmochim. Acta* **1997**, *61*, 4079–4094. DOI:10.1016/S0016-7037(97)00231-7
36. Baturin, G.N.; Yushina, I.G. Rare earth elements in phosphate-ferromanganese crusts on Pacific seamounts. *Lithol. Miner. Resour.* **2007**, *42 (2)*, 101–117. DOI:10.1134/S0024490207020010
37. Cui, Y., Shi, X., Liu, J., Ren, X. Effects of phosphatization on the elemental association of cobalt-rich crusts. *Bull. Geol. Sci. Tech*. **2008**, *27*, 61–67. DOI: 10.1111/j.1755-6724.2005.tb00900.x
38. Ren, J.; He, G.; Yao, H.; Deng, X.; Zhu, K.; Yang, S. The effects of phosphatization on the REY of Co-rich Fe-Mn crusts. *Mar. Geol. Quat. Geol.* **2017**, *37(2)*, 33–43. DOI: 10.16562/j.cnki.0256-1492.2017.02.004
39. Martini, E.; Worsley, T. Standard Neogene calcareous nannoplankton zonation. *Nature* **1970**, *225*, 289–290.
40. Martini, E. Standard Tertiary and Quaternary calcareous nannoplankton zonation. In: Farinacci, A. (Ed.) *Proc. 2nd Planktonic Conference*; Edizioni Tecnoscienza: Bologna, Italy, **1971,** *2*, 1225–1230.
41. Bukry, D. Biostratigraphy of Cenozoic marine sediment by calcareous nannofossils. *Micropaleontology* **1978**, *24(1)*, 44–60.
42. Okada, H.; Bukry, D. Supplementary modification and introduction of code numbers to the low latitude coccolith biostratigraphic zonation. *Mar. Micropaleontol.* **1980**, *5*, 321–325. DOI:10.1016/0377-8398(80)90016-X
43. Koschinsky, A.; Hein, J.R. Marine Ferromanganese Encrustations: Archives of Changing Oceans. *Elements* **2017**, *13*, 177–182. DOI:10.2113/gselements.13.3.177
44. Hein, J.R.; Koschinsky, A. Deep-ocean ferromanganese crusts and nodules. *Treatise Geochem*. **2014**, *13*, 273–291. DOI:10.1016/B978-0-08-095975-7.01111-6
45. Glasby, G.P.; Ren, X.; Shi, X.; Pulyaeva, I.A. Co-rich Mn crusts from the Magellan seamounts cluster: The long journey through time. *Geo-Mar Lett.* **2007**, *27*, 315–323. DOI: 10.1007/s00367-007-0055-5
46. Koschinsky, A.; Hein, J. Acquisition of elements from seawater by ferromanganese crusts: Solid phase associations and seawater speciation. *Mar. Geol.* **2003**, *19*, 331–351. DOI:10.1016/S0025-3227(03)00122-1
47. Melnikov, M.E.; Pletnev S.P. Distribution of cerium in accumulations of manganese crusts of different ranks on the Magellan seamount (Pacific Ocean). *Geology and minerals of the world ocean* **2009**, *1*, 23–26. (In Russian)
48. Asavin, A.M.; Kubrakova, I.V.; Melnikov, M.E.; Tyutyunnik, O.A.; Chesalova, E.I. Geochemical zoning in ferromanganese crusts of Ita-Mai-Tai guyot. *Geochem. Int.* **2010**, *48 (5)*, 423–445. DOI: 10.1134/S0016702910050010
49. Yang, K.; Ma, W.; Zhang, W.; Li, Z.; He, G.; Li, X.; Qiu, Z.; Wang, H.; Zhao, B.; Yang, Y.; Wei, Z.; Liu, Y. Geological and geochemical characteristics of shallow-buried ferromanganese crusts from Weijia Guyot and their resource potential. *Marine Geol.*, **2023**, *464(5)*:107119. DOI:10.1016/j.margeo.2023.107119
50. Novikov, G.V.; Melnikov, M.E.; Bogdanova, O.Y.; Drozdova, A.N.; Lobus, N.V. Mineralogy and geochemistry of Co-bearing manganese crusts from the Govorov and Volcanologist guyots of the Magellan Seamounts (Pacific Ocean). *Oceanology* **2017**. 57 (5), 716–722. DOI:10.1134/S0001437017050137
51. Novikov, G.V.; Lobkovsky, L.I.; Lobusa, N.V.; Bogdanova, O.Y; Sedysheva, T.E. Ore content of Co-rich ferromanganese crust of the Govorov guyot of the Magellanic mountains of the Pacific Ocean. *Dokl. Earth Sci.* **2021**, *499(2)*, 675–682. DOI: 10.31857/S2686739721080090
52. Novikov, G.V.; Sedysheva, T.E.; Bogdanova, O.Yu.; Lobus, N.V. Cobalt-rich ferromanganese crusts of the Kotzebue guyot of the Magellan seamount of the Pacific Ocean: conditions of occurrence, mineralogy, and geochemistry. *Oceanology* **2022,** *62 (6)*, 879–889. DOI:10.1134/S0001437022050162
53. Yang, K.; Park, H.; Son, S.K.; Baik, H.; Park, K.; Kim, J.; Yoon, J.; Park, C.H.; Kim, J. Electron microscopy study on the formation of ferromanganese crusts, western Pacific Magellan Seamounts. *Mar. Geol.* **2019**, *410*, 32–41. DOI:10.1016/j.margeo.2019.01.001
54. Wang, L.; Zeng, Z. The geochemical features and genesis of ferromanganese deposits from Caiwei Guyot, Northwestern Pacific Ocean. *J. Mar. Sci. Eng*. **2022**, *10*, 1275. DOI:10.3390/jmse10091275
55. Yang, Y.; Xiao, B.; Shi, X.; Zhang, S. Unusual cobalt behaviors and enrichment in cobalt-rich crust from the Magellan seamounts in the Western Pacific. *Ore Geol. Rev.* **2024**, *173*:106234. DOI:10.1016/j.oregeorev.2024.106234

56. Park, J.; Hwang, H.; An, Y.; Yang, K. High-resolution reconstruction of oxidation–reduction conditions: Raman spectroscopy and μ-XRF analysis of manganese nodule and crust on tabletop of Western Pacific Magellan Seamounts. *Minerals* **2024**, *14*, 1135. DOI:10.3390/min14111135
57. Dubinin, A.V. *Geochemistry of Rare-Earth Elements in the Ocean;* Nauka: Moscow, Russia, 2006; 360p. (In Russian)
58. McLennan, S.M. Rare earth elements in sedimentary rocks; influence of provenance and sedimentary processes. In: Lipin, B.R.; McKay, G.A. (Eds.), *Geochemistry and Mineralogy of Rare Earth Elements.* De Gruyter, Berlin. **1989;** 169–200. DOI:10.1515/9781501509032-010
59. Bonatti, E.; Kraemer, T.; Rydell, H. Classification and genesis of submarine iron-manganese deposits. *In:* Horn, D.R. (Ed.) *Ferromanganese Deposits on the Sea Floor;* Arden House; Harriman: New York, 1972; 149p.
60. Halbach, P.; Scherhag, C.; Hebisch, U.; Marchig, V. Geochemical and mineralogical control of different genetic types of deep-sea nodules from the Pacifc Ocean. *Mineral. Deposita* **1981**, *16 (1)*, 59–84. DOI:10.1007/BF00206455
61. Josso, P.; Pelleter, E.; Pourret, O.; Fouquet, Y.; Etoubleau, J.; Cheron, S.; Bollinger, C. A new discrimination scheme for oceanic ferromanganese deposits using high field strength and rare earth elements. *Ore Geol. Rev.* **2017**, *87*, 3–15. DOI:10.1016/j.oregeorev.2016.09.003
62. Bau, M.; Schmidt, K.; Koschinsky, A.; Hein, J.; Kuhn, T.; Usui, A. Discriminating between different genetic types of marineferro-manganese crusts and nodules based on rare earth elements and yttrium. *Chem. Geol*. **2014**, *381*, 1–9. DOI:10.1016/j.chemgeo.2014.05.004
63. Deng, X.; Liu, Y;, Luo, J.; Hu, G.; Wang, W.; Deng, X.; Wang, H.; Wei, Z.; Ren, J.; Zhou, J. Effects of phosphatization on the mineralogical and geochemical composition of marine ferromanganese crusts from the JiaXie Guyot in the Western Pacific: Constraints from high resolution analysis. *Ore Geol. Rev*. **2024**, *172*: 106209. DOI:10.1016/j.oregeorev.2024.106209
64. Jiang, X.D.; Sun, X.M.; Chou, Y.M.; Hein, J.R.; He, G.W.; Fu, Y.; Li, D.F.; Liao, J.L.; Ren, J.B. Geochemistry and origins of carbonate fluorapatite in seamount Fe-Mn crusts from the Pacific Ocean. *Mar. Geol.* **2020**, *423*, 106135. DOI:10.1016/j.margeo.2020.106135
65. Bau, M.; Koshcinsky, A. Oxidative scavenging of cerium on hydrous Fe oxide: Evidence from the distribution of rare earth elements and yttrium between Fe oxides and Mn oxides in hydrogenetic ferromanganese crusts. *Geochem. J.* **2009**, *43 (1)*, 37–47. DOI: 10.2343/geochemj.1.00052009
66. Claude, C.; Suhr, G.; Hofmann, A.W.; Koschinsky, A. U-Th chronology and paleoceanographic record in a Fe-Mn crust from the NE Atlantic over the last 700 ka. *Geochim. Cosmochim. Acta* **2005,** *69(20)*. 4845–4854. DOI: 10.1016/j.gca.2005.05.016
67. Josso, P.; Parkinson, I.; Horstwood, M.; Lusty, P.; Chenery, S.; Murton, B. Improving confidence in ferromanganese crust age models: A composite geochemical approach. *Chem. Geol*. **2019**, *513*, 108–119. DOI:10.1016/j.chemgeo.2019.03.003
68. Klemm, V.; Levasseur, S.; Frank, M.; Hein, J.R.; Halliday, A.N. Osmium isotope stratigraphy of a marine ferromanganese crust. *Earth Planet. Sci. Lett.* **2005**, *238*, 42–48. DOI:10.1016/j.chemgeo.2019.03.003
69. Goto, K.T.; Anbar, A.D.; Gordon, G.W.; Romaniello, S.J.; Shimoda, G.; Takaya, Y.; Tokumaru, A.; Nozaki, T.; Suzuki, K.; Machida, M.; Hanyu, T.; Usui, A. Uranium isotope systematics of ferromanganese crusts in the Pacific Ocean: Implications for the marine $^{238}U/^{235}U$ isotope system. *Geochim. Cosmochim. Acta* **2014,** *146(20)*. 43-58. DOI:10.1016/j.gca.2014.10.003
70. Zeng, X.; Zhang, J.; Yao, H.; Ren, J.; Li, J. A high-resolution Os-Nd-Pb isotopic record of a hydrogenous Fe–Mn crust from the Northwestern Pacific and its response to plate motion. *Mar. Geol.* **2023**, *459*, 107028. DOI:10.1016/j.margeo.2023.107028
71. Peng, J.; Li, D.; Poulton, S.W.; O'Sullivan G.J.; Chew, D.; Yu Fu, Y.; Sun, X. Episodic intensification of marine phosphorus burial over the last 80 million years. *Nat. Com.* **2024,** 15:7446. DOI:10.1038/s41467-024-51598-x
72. Puteanus, D.; Halbach, P. Correlation of Co concentration and growth rate — a method for age determination of ferromanganese crusts. *Chem. Geol.* **1988**, *69*, 73–85. DOI:10.1016/0009-2541(88)90159-3
73. Halbach, P.; Segl, M.; Puteanus, D.; Mangini, A. Co-fluxes and growth rates in ferromanganese deposits from central Pacific seamount areas. *Nature* **1983**, *304*, 716-719. DOI:10.1038/304716a0

 doi:10.20944/preprints202510.1578.v1

74. Manheim, F.T.; Lane-Bostwick, C.M. Cobalt in ferromanganese crusts as a monitor of hydrothermal discharge on the Pacific sea floor. *Nature* **1988**, *335*, 59–62. DOI:10.1038/335059a0